

Fermi National Accelerator Laboratory

FERMILAB Pub-96/216-E
CDF

**Measurement of $b\bar{b}$ Production Correlations,
 $B^0\bar{B}^0$ Mixing, and a Limit on ε_B in $p\bar{p}$ Collisions
at $\sqrt{s} = 1.8$ TeV**

F. Abe et al.
The CDF Collaboration

*Fermi National Accelerator Laboratory
P.O. Box 500, Batavia, Illinois 60510-0500*

August 1996

Submitted to *Physical Review D*
August 8, 1996

Disclaimer

This report was prepared as an account of work sponsored by an agency of the United States Government. Neither the United States Government nor any agency thereof, nor any of their employees, makes any warranty, express or implied, or assumes any legal liability or responsibility for the accuracy, completeness or usefulness of any information, apparatus, product or process disclosed, or represents that its use would not infringe privately owned rights. Reference herein to any specific commercial product, process or service by trade name, trademark, manufacturer or otherwise, does not necessarily constitute or imply its endorsement, recommendation or favoring by the United States Government or any agency thereof. The views and opinions of authors expressed herein do not necessarily state or reflect those of the United States Government or any agency thereof.

Distribution

Approved for public release: further dissemination unlimited.

Measurement of $b\bar{b}$ Production Correlations, $B^0\bar{B}^0$ Mixing, and a Limit on ϵ_B in $p\bar{p}$ Collisions at $\sqrt{s} = 1.8$ TeV

F. Abe,¹⁵ H. Akimoto,³³ A. Akopian,²⁸ M. G. Albrow,⁷ S. R. Amendolia,²⁴ D. Amidei,¹⁸
J. Antos,³⁰ C. Anway-Wiese,⁴ S. Aota,³³ G. Apollinari,²⁸ T. Asakawa,³³ W. Ashmanskas,¹⁶
M. Atac,⁷ F. Azfar,²³ P. Azzi-Bacchetta,²² N. Bacchetta,²² W. Badgett,¹⁸ S. Bagdasarov,²⁸
M. W. Bailey,²⁰ J. Bao,³⁶ P. de Barbaro,²⁷ A. Barbaro-Galtieri,¹⁶ V. E. Barnes,²⁶
B. A. Barnett,¹⁴ E. Barzi,⁸ G. Bauer,¹⁷ T. Baumann,¹⁰ F. Bedeschi,²⁴ S. Behrends,³
S. Belforte,²⁴ G. Bellettini,²⁴ J. Bellinger,³⁵ D. Benjamin,³² J. Benlloch,¹⁷ J. Bensinger,³
D. Benton,²³ A. Beretvas,⁷ J. P. Berge,⁷ J. Berryhill,⁵ S. Bertolucci,⁸ B. Bevensee,²³
A. Bhatti,²⁸ K. Biery,¹³ M. Binkley,⁷ D. Bisello,²² R. E. Blair,¹ C. Blocker,³ A. Bodek,²⁷
W. Bokhari,¹⁷ V. Bolognesi,² G. Bolla,²² D. Bortoletto,²⁶ J. Boudreau,²⁵ L. Breccia,²
C. Bromberg,¹⁹ N. Bruner,²⁰ E. Buckley-Geer,⁷ H. S. Budd,²⁷ K. Burkett,¹⁸ G. Busetto,²²
A. Byon-Wagner,⁷ K. L. Byrum,¹ J. Cammerata,¹⁴ C. Campagnari,⁷ M. Campbell,¹⁸
A. Caner,²⁴ W. Carithers,¹⁶ D. Carlsmith,³⁵ A. Castro,²² D. Cauz,²⁴ Y. Cen,²⁷ F. Cervelli,²⁴
P. S. Chang,³⁰ P. T. Chang,³⁰ H. Y. Chao,³⁰ J. Chapman,¹⁸ M. -T. Cheng,³⁰ G. Chiarelli,²⁴
T. Chikamatsu,³³ C. N. Chiou,³⁰ L. Christofek,¹² S. Cihangir,⁷ A. G. Clark,⁹ M. Cobal,²⁴
E. Cocca,²⁴ M. Contreras,⁵ J. Conway,²⁹ J. Cooper,⁷ M. Cordelli,⁸ C. Couyoumtzelis,⁹
D. Crane,¹ D. Cronin-Hennessy,⁶ R. Culbertson,⁵ T. Daniels,¹⁷ F. DeJongh,⁷ S. Delchamps,⁷
S. Dell'Agnello,²⁴ M. Dell'Orso,²⁴ R. Demina,⁷ L. Demortier,²⁸ B. Denby,²⁴ M. Deninno,²
P. F. Derwent,⁷ T. Devlin,²⁹ J. R. Dittmann,⁶ S. Donati,²⁴ J. Done,³¹ T. Dorigo,²²
A. Dunn,¹⁸ N. Eddy,¹⁸ K. Einsweiler,¹⁶ J. E. Elias,⁷ R. Ely,¹⁶ E. Engels, Jr.,²⁵ D. Errede,¹²
S. Errede,¹² Q. Fan,²⁶ C. Ferretti,²⁴ I. Fiori,² B. Flaughner,⁷ G. W. Foster,⁷ M. Franklin,¹⁰
M. Frautschi,³² J. Freeman,⁷ J. Friedman,¹⁷ T. A. Fuess,¹ Y. Fukui,¹⁵ S. Funaki,³³
G. Gagliardi,²⁴ S. Galeotti,²⁴ M. Gallinaro,²² M. Garcia-Sciveres,¹⁶ A. F. Garfinkel,²⁶
C. Gay,¹⁰ S. Geer,⁷ D. W. Gerdes,¹⁴ P. Giannetti,²⁴ N. Giokaris,²⁸ P. Giromini,⁸ G. Giusti,²⁴
L. Gladney,²³ D. Glenzinski,¹⁴ M. Gold,²⁰ J. Gonzalez,²³ A. Gordon,¹⁰ A. T. Goshaw,⁶

K. Goulianos,²⁸ H. Grassmann,²⁴ L. Groer,²⁹ C. Grosso-Pilcher,⁵ G. Guillian,¹⁸ R. S. Guo,³⁰ C. Haber,¹⁶ E. Hafen,¹⁷ S. R. Hahn,⁷ R. Hamilton,¹⁰ R. Handler,³⁵ R. M. Hans,³⁶ K. Hara,³³ A. D. Hardman,²⁶ B. Harral,²³ R. M. Harris,⁷ S. A. Hauger,⁶ J. Hauser,⁴ C. Hawk,²⁹ E. Hayashi,³³ J. Heinrich,²³ K. D. Hoffman,²⁶ M. Hohlmann,⁵ C. Holck,²³ R. Hollebeek,²³ L. Holloway,¹² A. Hölscher,¹³ S. Hong,¹⁸ G. Houk,²³ P. Hu,²⁵ B. T. Huffman,²⁵ R. Hughes,²⁷ J. Huston,¹⁹ J. Huth,¹⁰ J. Hysten,⁷ H. Ikeda,³³ M. Incagli,²⁴ J. Incandela,⁷ G. Introzzi,²⁴ J. Iwai,³³ Y. Iwata,¹¹ H. Jensen,⁷ U. Joshi,⁷ R. W. Kadel,¹⁶ E. Kajfasz,²² H. Kambara,⁹ T. Kamon,³¹ T. Kaneko,³³ K. Karr,³⁴ H. Kasha,³⁶ Y. Kato,²¹ T. A. Keaffaber,²⁶ L. Keeble,⁸ K. Kelley,¹⁷ R. D. Kennedy,²⁹ R. Kephart,⁷ P. Kesten,¹⁶ D. Kestenbaum,¹⁰ R. M. Keup,¹² H. Keutelian,⁷ F. Keyvan,⁴ B. Kharadia,¹² B. J. Kim,²⁷ D. H. Kim,^{7a} H. S. Kim,¹³ S. B. Kim,¹⁸ S. H. Kim,³³ Y. K. Kim,¹⁶ L. Kirsch,³ P. Koehn,²⁷ K. Kondo,³³ J. Konigsberg,¹⁰ S. Kopp,⁵ K. Kordas,¹³ A. Korytov,¹⁷ W. Koska,⁷ E. Kovacs,^{7a} W. Kowald,⁶ M. Krasberg,¹⁸ J. Kroll,⁷ M. Kruse,²⁷ T. Kuwabara,³³ S. E. Kuhlmann,¹ E. Kuns,²⁹ A. T. Laasanen,²⁶ N. Labanca,²⁴ S. Lammel,⁷ J. I. Lamoureux,³ T. LeCompte,¹ S. Leone,²⁴ J. D. Lewis,⁷ P. Limon,⁷ M. Lindgren,⁴ T. M. Liss,¹² N. Lockyer,²³ O. Long,²³ C. Loomis,²⁹ M. Loreti,²² J. Lu,³¹ D. Lucchesi,²⁴ P. Lukens,⁷ S. Lusin,³⁵ J. Lys,¹⁶ K. Maeshima,⁷ A. Maghakian,²⁸ P. Maksimovic,¹⁷ M. Mangano,²⁴ J. Mansour,¹⁹ M. Mariotti,²² J. P. Marriner,⁷ A. Martin,¹² J. A. J. Matthews,²⁰ R. Mattingly,¹⁷ P. McIntyre,³¹ P. Melese,²⁸ A. Menzione,²⁴ E. Meschi,²⁴ S. Metzler,²³ C. Miao,¹⁸ T. Miao,⁷ G. Michail,¹⁰ R. Miller,¹⁹ H. Minato,³³ S. Miscetti,⁸ M. Mishina,¹⁵ H. Mitsushio,³³ T. Miyamoto,³³ S. Miyashita,³³ N. Moggi,²⁴ Y. Morita,¹⁵ J. Mueller,²⁵ A. Mukherjee,⁷ T. Muller,⁴ P. Murat,²⁴ H. Nakada,³³ I. Nakano,³³ C. Nelson,⁷ D. Neuberger,⁴ C. Newman-Holmes,⁷ M. Ninomiya,³³ L. Nodulman,¹ S. H. Oh,⁶ K. E. Ohl,³⁶ T. Ohmoto,¹¹ T. Ohsugi,¹¹ R. Oishi,³³ M. Okabe,³³ T. Okusawa,²¹ R. Oliveira,²³ J. Olsen,³⁵ C. Pagliarone,² R. Paoletti,²⁴ V. Papadimitriou,³² S. P. Pappas,³⁶ S. Park,⁷ A. Parri,⁸ J. Patrick,⁷ G. Pauletta,²⁴ M. Paulini,¹⁶ A. Perazzo,²⁴ L. Pescara,²² M. D. Peters,¹⁶ T. J. Phillips,⁶ G. Piacentino,² M. Pillai,²⁷ K. T. Pitts,⁷ R. Plunkett,⁷ L. Pondrom,³⁵ J. Proudfoot,¹ F. Ptohos,¹⁰ G. Punzi,²⁴ K. Ragan,¹³ A. Ribon,²² F. Rimondi,² L. Ristori,²⁴ W. J. Robertson,⁶ T. Rodrigo,²⁴ S. Rolli,²⁴

J. Romano,⁵ L. Rosenson,¹⁷ R. Roser,¹² W. K. Sakumoto,²⁷ D. Saltzberg,⁵ A. Sansoni,⁸
L. Santi,²⁴ H. Sato,³³ P. Schlabach,⁷ E. E. Schmidt,⁷ M. P. Schmidt,³⁶ A. Scribano,²⁴
S. Segler,⁷ S. Seidel,²⁰ Y. Seiya,³³ G. Sganos,¹³ M. D. Shapiro,¹⁶ N. M. Shaw,²⁶ Q. Shen,²⁶
P. F. Shepard,²⁵ M. Shimojima,³³ M. Shochet,⁵ J. Siegrist,¹⁶ A. Sill,³² P. Sinervo,¹³ P. Singh,²⁵
J. Skarha,¹⁴ K. Sliwa,³⁴ F. D. Snider,¹⁴ T. Song,¹⁸ J. Spalding,⁷ T. Speer,⁹ P. Sphicas,¹⁷
F. Spinella,²⁴ M. Spiropulu,¹⁰ L. Spiegel,⁷ L. Stanco,²² J. Steele,³⁵ A. Stefanini,²⁴ K. Strahl,¹³
J. Strait,⁷ R. Ströhmer,^{7^a} D. Stuart,⁷ G. Sullivan,⁵ A. Soumarokov,³⁰ K. Sumorok,¹⁷
J. Suzuki,³³ T. Takada,³³ T. Takahashi,²¹ T. Takano,³³ K. Takikawa,³³ N. Tamura,¹¹
F. Tartarelli,²⁴ W. Taylor,¹³ P. K. Teng,³⁰ Y. Teramoto,²¹ S. Tether,¹⁷ D. Theriot,⁷
T. L. Thomas,²⁰ R. Thun,¹⁸ M. Timko,³⁴ P. Tipton,²⁷ A. Titov,²⁸ S. Tkaczyk,⁷ D. Toback,⁵
K. Tollefson,²⁷ A. Tollestrup,⁷ J. F. de Troconiz,¹⁰ S. Truitt,¹⁸ J. Tseng,¹⁴ N. Turini,²²
T. Uchida,³³ N. Uemura,³³ F. Ukegawa,²³ G. Unal,²³ J. Valls,^{7^a} S. C. van den Brink,²⁵
S. Vejcik, III,¹⁸ G. Velev,²⁴ R. Vidal,⁷ M. Vondracek,¹² D. Vucinic,¹⁷ R. G. Wagner,¹
R. L. Wagner,⁷ J. Wahl,⁵ N. Wallace,²⁴ C. Wang,⁶ C. H. Wang,³⁰ J. Wang,⁵ M. J. Wang,³⁰
Q. F. Wang,²⁸ A. Warburton,¹³ T. Watts,²⁹ R. Webb,³¹ C. Wei,⁶ C. Wendt,³⁵ H. Wenzel,¹⁶
W. C. Wester, III,⁷ A. B. Wicklund,¹ E. Wicklund,⁷ R. Wilkinson,²³ H. H. Williams,²³
P. Wilson,⁵ B. L. Winer,²⁷ D. Winn,¹⁸ D. Wolinski,¹⁸ J. Wolinski,¹⁹ S. Worm,²⁰ X. Wu,⁹
J. Wyss,²² A. Yagil,⁷ W. Yao,¹⁶ K. Yasuoka,³³ Y. Ye,¹³ G. P. Yeh,⁷ P. Yeh,³⁰ M. Yin,⁶
J. Yoh,⁷ C. Yosef,¹⁹ T. Yoshida,²¹ D. Yovanovitch,⁷ I. Yu,⁷ L. Yu,²⁰ J. C. Yun,⁷ A. Zanetti,²⁴
F. Zetti,²⁴ L. Zhang,³⁵ W. Zhang,²³ and S. Zucchelli²

(CDF Collaboration)

¹ *Argonne National Laboratory, Argonne, Illinois 60439*

² *Istituto Nazionale di Fisica Nucleare, University of Bologna, I-40126 Bologna, Italy*

³ *Brandeis University, Waltham, Massachusetts 02254*

⁴ *University of California at Los Angeles, Los Angeles, California 90024*

⁵ *University of Chicago, Chicago, Illinois 60637*

- ⁶ *Duke University, Durham, North Carolina 27708*
- ⁷ *Fermi National Accelerator Laboratory, Batavia, Illinois 60510*
- ⁸ *Laboratori Nazionali di Frascati, Istituto Nazionale di Fisica Nucleare, I-00044 Frascati, Italy*
- ⁹ *University of Geneva, CH-1211 Geneva 4, Switzerland*
- ¹⁰ *Harvard University, Cambridge, Massachusetts 02138*
- ¹¹ *Hiroshima University, Higashi-Hiroshima 724, Japan*
- ¹² *University of Illinois, Urbana, Illinois 61801*
- ¹³ *Institute of Particle Physics, McGill University, Montreal H3A 2T8, and University of Toronto,
Toronto M5S 1A7, Canada*
- ¹⁴ *The Johns Hopkins University, Baltimore, Maryland 21218*
- ¹⁵ *National Laboratory for High Energy Physics (KEK), Tsukuba, Ibaraki 305, Japan*
- ¹⁶ *Ernest Orland Lawrence Berkeley Laboratory, Berkeley, California 94720*
- ¹⁷ *Massachusetts Institute of Technology, Cambridge, Massachusetts 02139*
- ¹⁸ *University of Michigan, Ann Arbor, Michigan 48109*
- ¹⁹ *Michigan State University, East Lansing, Michigan 48824*
- ²⁰ *University of New Mexico, Albuquerque, New Mexico 87131*
- ²¹ *Osaka City University, Osaka 588, Japan*
- ²² *Universita di Padova, Istituto Nazionale di Fisica Nucleare, Sezione di Padova, I-35131 Padova, Italy*
- ²³ *University of Pennsylvania, Philadelphia, Pennsylvania 19104*
- ²⁴ *Istituto Nazionale di Fisica Nucleare, University and Scuola Normale Superiore of Pisa, I-56100 Pisa, Italy*
- ²⁵ *University of Pittsburgh, Pittsburgh, Pennsylvania 15260*
- ²⁶ *Purdue University, West Lafayette, Indiana 47907*
- ²⁷ *University of Rochester, Rochester, New York 14627*
- ²⁸ *Rockefeller University, New York, New York 10021*
- ²⁹ *Rutgers University, Piscataway, New Jersey 08854*
- ³⁰ *Academia Sinica, Taipei, Taiwan 11529, Republic of China*
- ³¹ *Texas A&M University, College Station, Texas 77843*
- ³² *Texas Tech University, Lubbock, Texas 79409*

³³ *University of Tsukuba, Tsukuba, Ibaraki 305, Japan*

³⁴ *Tufts University, Medford, Massachusetts 02155*

³⁵ *University of Wisconsin, Madison, Wisconsin 53706*

³⁶ *Yale University, New Haven, Connecticut 06511*

Abstract

We present measurements of correlated $b\bar{b}$ cross sections, $\mu - \mu$ correlations, the average $B^0\bar{B}^0$ mixing parameter $\bar{\chi}$, and a limit on the CP violating parameter ϵ_B . For these measurements, we use muon pairs from $b\bar{b}$ double semileptonic decays. The data used in this analysis were taken with the Collider Detector at Fermilab and represent an integrated luminosity of 17.4 ± 0.6 pb⁻¹. The results concerning $b\bar{b}$ production correlations are compared to predictions of next-to-leading order QCD computations.

PACS numbers: 13.85.Qk, 13.20.Jf

I. INTRODUCTION

Production of b quarks in high energy $p\bar{p}$ collisions constitutes a useful process for the study of perturbative QCD. The cross section for inclusive b quark production at $\sqrt{s} = 1.8$ TeV has been measured using semileptonic decays of B hadrons and exclusive B meson decays [1–3]. The results of these measurements are systematically higher than the next-to-leading order (NLO) QCD prediction.

A recent measurement of the $\mu - \bar{b}$ cross section [4] has given valuable information on the production of a pair of b quarks. The $\mu - \bar{b}$ cross section has been measured as a function of the \bar{b} jet transverse energy ($E_T = E \sin \theta$ where θ is the polar angle from the proton beam), the \bar{b} transverse momentum, and the azimuthal opening angle between the μ and the \bar{b} jet. In addition to a higher value, the $\mu - \bar{b}$ cross sections show some qualitative differences in the shapes between the measurement and the NLO QCD prediction on $b\bar{b}$ production. Thus, another independent study of $b\bar{b}$ production is important to test the NLO QCD calculation. In this paper, $b\bar{b}$ production is studied using dimuon events in which each muon comes from a b decay. These results provide information on the production of $b\bar{b}$ pairs [5] with lower transverse momentum values for the bottom quarks ($P_T(\bar{b}) = 6 - 12$ GeV/c) than the $\mu - \bar{b}$ cross section measurement ($P_T(\bar{b}) = 25 - 80$ GeV/c).

$B\bar{B}$ hadron pairs generated by the fragmentation of $b\bar{b}$ pairs may also be used to study the weak interaction phenomena of $B^0\bar{B}^0$ mixing and CP violation. Measurements of $B^0\bar{B}^0$ mixing can be used to impose constraints on elements of the Cabibbo-Kobayashi-Maskawa matrix [6]. Studies of CP violation in the B system are of fundamental importance in understanding the Standard Model. As an extension of the $b\bar{b}$ production correlation analysis, we also report on a measurement of $B^0\bar{B}^0$ mixing and a limit on CP violation in $B^0\bar{B}^0$ mixing.

In the CDF experiment, dimuon events result from decays of heavy quark pairs ($t\bar{t}$, $b\bar{b}$, $c\bar{c}$), the Drell-Yan process, charmonium and bottomonium decays, and decays of π or K mesons. Background in these dimuon events also comes from the misidentification of π and K as muons. We make use of the precision tracking provided by the CDF silicon vertex

detector to identify muons from B decays. The long lifetime of B hadrons [7–10], coupled with the precision tracking, enables separation of $b\bar{b}$ events from the background events. Specifically, the impact parameter (to be defined in Section IV) of a muon track is used to determine the $b\bar{b}$ content of the dimuon events. We measure the integral cross section for $b\bar{b}$ production as a function of $P_T(\bar{b})$. The production correlations of a muon pair from $b\bar{b}$ decay are also studied by examining the distribution of the opening angle between the muons and the muon P_T distribution. A comparison of the number of $b\bar{b}$ events with like-sign (LS) and opposite-sign (OS) dimuons yields a value of the average $B^0\bar{B}^0$ mixing parameter, $\bar{\chi}$. In addition, the asymmetry between the number of $\mu^+\mu^+$ and $\mu^-\mu^-$ events is used to place a limit on the real part of ϵ_B which gives rise to CP violation in $B^0\bar{B}^0$ mixing [11].

Sections II and III describe the detector systems relevant to the analysis and the data selection, respectively. The method used for the measurements is discussed in Section IV. The results of the $b\bar{b}$ production correlation measurements are presented in Sections V and VI. In Sections VII and VIII, we describe the results of the mixing and the CP violation analyses. Section IX closes with a discussion of the experimental results and a comparison with the theoretical predictions.

II. DETECTOR

In CDF, the proton beam direction defines the z axis, r is the radius in the plane transverse to the beam, ϕ is the azimuthal angle, and θ is the polar angle with respect to the proton direction. The pseudorapidity η is defined as $\eta \equiv -\ln \tan(\theta/2)$. In this section, we describe subsystems of the CDF detector relevant to the analysis. More details and descriptions of other detector components can be found in [12].

A. Tracking System

The CDF central tracking system consists of a solenoid magnet with a field of 1.4 Tesla containing 3 main detectors: the silicon vertex detector (SVX) [13], the vertex time projec-

tion chamber (VTX), and the central tracking chamber (CTC) [14]. Closest to the beam line, the SVX consists of four layers of silicon strip detectors extending ± 27.3 cm in z from the center of the detector. The SVX is designed to provide precision tracking in the $r - \phi$ plane. The innermost layer is located at a radius of 2.9 cm and has a spatial resolution of $13 \mu\text{m}$. Surrounding the SVX is the VTX, a time projection chamber consisting of 28 modules and covering the pseudorapidity region $|\eta| \leq 3.5$. At the Tevatron, $p\bar{p}$ interactions occur along the beam axis according to a Gaussian distribution with width of 27 cm. The VTX allows the determination of the interaction vertex position in z with a resolution of 1 mm. The CTC is a cylindrical drift chamber which provides three dimensional tracking measurements for charged particles. The CTC consists of 84 layers of sense wires grouped into 9 superlayers and covers radii from 28 cm to 132 cm. The momentum resolution of the CTC is $\delta P_T/P_T = 0.002P_T$ where P_T , defined to be $P \sin \theta$, is in GeV/c. For a charged particle track reconstructed in both the CTC and SVX, the P_T of the track is determined with the improved momentum resolution of $\delta P_T/P_T = \sqrt{(0.0009P_T)^2 + (0.0066)^2}$.

B. Muon System

Muon candidates are identified by two different subsystems in the central region ($|\eta| \leq 0.6$). The central muon system (CMU) [15] is located behind 5 absorption lengths of material and consists of four layers of drift chambers covering about 84% of the solid angle for $|\eta| \leq 0.6$. The central muon upgrade system (CMP) [16] is located behind an additional 3 absorption lengths of material, covers 63% of the solid angle for $|\eta| \leq 0.6$, and significantly reduces misidentification of hadrons as muons. About 53% of the solid angle for $|\eta| \leq 0.6$ is covered by both systems. A set of more than 2 hits in radially adjacent wires in a muon detector is identified as a muon track segment and its momentum is measured using the CTC track extrapolated to the muon track segment.

C. Trigger

CDF collects data using a three-level trigger system. The data used in this analysis were collected with a dimuon trigger. The Level 1 central dimuon trigger requires two muon track segments in the CMU with P_T greater than 3 GeV/c. At Level 1, the P_T of a muon track segment is roughly measured using the drift time difference between layers in the CMU. The Level 2 trigger requires at least one of the two muon track segments to match a track in the CTC as found by the Central Fast Tracker (CFT) [17], a hardware track processor. The CFT determines the P_T of a charged track with a momentum resolution of $\delta P_T/P_T = 0.035 P_T$. The trigger requires the muon track segment and a CTC track with $P_T \geq 3$ GeV/c to lie within $\Delta\phi \leq 15^\circ$. In addition the hadronic energy deposition in the calorimeter tower pointing to the muon segment is required to be greater than 0.5 GeV, as expected for a minimum ionizing particle. The Level 3 trigger performs full event reconstruction. At Level 3, the dimuon trigger requires two CMU muon segments, each of which is matched to a CTC track which has been fully reconstructed in 3 dimensions. The P_T of each muon track is required to be greater than 2 GeV/c at Level 3.

III. DATA SELECTION

Muons are selected in the analysis by requiring $P_T \geq 3$ GeV/c for each muon and a matching between the extrapolated CTC track and the muon segment within 3σ in the $r - \phi$ plane and $\sqrt{12}\sigma$ in z , where σ is a standard deviation including the effect of multiple scattering and energy loss. In addition a muon segment in the CMP chamber is required in order to minimize misidentification of muons due to hadronic punchthrough. In order to use the SVX precision tracking for muons, we require the event interaction vertex $|z_0| \leq 30$ cm. We also require the impact parameter of a muon track (to be defined in Section IV) to be less than 0.06 cm. With this impact parameter cut, we remove almost all of the cosmic ray events, which have a uniform impact parameter distribution. Dimuon events from cascade

decays of a b quark ($b \rightarrow \mu_1 c X$, $c \rightarrow \mu_2 Y$) and J/ψ decays are removed by requiring the dimuon invariant mass to be greater than $5 \text{ GeV}/c^2$. This data selection yields 4750 events corresponding to an integrated luminosity of $17.4 \pm 0.6 \text{ pb}^{-1}$

IV. IMPACT PARAMETER FITTING METHOD

The impact parameter, d , of a track is defined as the distance of closest approach to the primary interaction point (the beam line) in the transverse plane. For tracks coming from decays of long lived particles, $d = |\beta\gamma ct \sin(\delta)|$, where t is the proper decay time of the parent particle from which the track originates, δ is the decay angle of the daughter track with respect to the direction of the parent particle, and $\beta\gamma$ is a Lorentz boost factor. The position of the beam line is measured by averaging the $p\bar{p}$ interaction positions of data collected over periods during which the proton-antiproton beam profile is constant. The impact parameter of a daughter muon is proportional to the lifetime of the parent particle. The markedly different impact parameter distributions expected for muons from b decays, c decays, and other sources allows the parent fractions to be determined.

A. Fitting Procedure

In this section, we describe a method to determine the $b\bar{b}$ content of the data using the muon impact parameter. The procedure is to fit the observed impact parameter distributions in the dimuon data with the expected impact parameter distributions of muons from various sources.

After data selection, the main sources of reconstructed muons are semileptonic decays of bottom and charm hadrons, prompt decays of bottomonium, the Drell-Yan process and decays of π or K . The contributions of cosmic ray interactions and top quark production are found to be negligible in the data [18,19]. Monte Carlo methods are used to establish the impact parameter distributions for muons from b and c decays as shown in Figure 1. We use the ISAJET Monte Carlo program [20] to generate $b\bar{b}$ events, the CLEO Monte

Carlo program QQ [21] to decay B hadrons, and a full detector simulation of CDF to model the detector's response. Since lifetimes of bottom and charm hadrons ($c\tau_B \sim 450\mu\text{m}$ and $c\tau_D \sim 200\mu\text{m}$ [11]) are much greater than the impact parameter resolution of the SVX ($\sim 15\mu\text{m}$), the dominant factor determining the impact parameter distributions of muons from charm and bottom decays is the kinematics of the semileptonic decays, which is well described by the Monte Carlo simulation. The fraction of muons from sequential b decays ($b \rightarrow cX \rightarrow \mu Y$) is also determined by the Monte Carlo simulation. Muon tracks from decays of π or K are regarded as prompt tracks since the CDF track reconstruction algorithm removes decay muons from π or K with a large kink. The remaining muons have an impact parameter distribution similar to that of prompt tracks in jet data, as shown in Figure 2. The jet data is collected with a trigger that requires at least one jet with $E_T \geq 20$ GeV. Tracks in the jet data are mostly of prompt origin and the contribution of tracks from b and c decays is found to be small [19]. The impact parameter distribution of tracks in the jet data, plotted in Figure 1, is used to represent that of muons from prompt sources such as bottomonium and the Drell-Yan process.

Since there are two muons in an event, a fit is performed in the two dimensional space of impact parameters. Each axis represents the impact parameter of one of the two muons. The two dimensional impact parameter fitting technique exploits the fact that the impact parameters for each muon are independent uncorrelated variables. The two dimensional template distributions for each type of dimuon event are made by combining the relevant one-dimensional distributions.

A binned maximum log likelihood method is used in the fit. The likelihood, L , can be defined as follows:

$$L = \prod_i \prod_j (l_{ij}^{n(i,j)} e^{-l_{ij}} / n(i,j)!)$$

$$l_{ij} = f_{bb} H_{bb}(i,j) + f_{pp} H_{pp}(i,j) + f_{sum} H_{sum}(i,j)$$

where $n(i,j)$ is the number of events in the (i,j) th bin. H_{bb} and H_{pp} represent normalized two dimensional impact parameter distributions for $b\bar{b}$ and prompt dimuon events, respec-

tively, and f 's are the corresponding fractions of each component. The template distribution, H_{sum} , is formed from the sum of the $c\bar{c}$ component, H_{cc} , (both muons from c decay) and the component, H_{bp} , representing events with one prompt muon from the decay of a π or a K and one muon from a b decay. With our statistical accuracy, these two components can not be extracted separately from a simultaneous fit since the distributions are similar to each other as shown in Figure 3. The relative fraction of the two components in H_{sum} is set to be equal and variations of f_{bb} due to different relative fractions are included in the systematic uncertainty. The two dimensional template histograms for each component in the likelihood are shown in Figure 4.

We perform the unconstrained fit to the data with $P_T \geq 3$ GeV/c for both muons and obtain 2471 ± 104 $b\bar{b}$ events, 1628 ± 188 prompt dimuon events and 652 ± 157 H_{sum} events, where the errors represent the 1σ uncertainty of the fit corresponding to a change in the log likelihood of 0.5. For a comparison of the data and the fit result, projections of the two dimensional impact parameter distributions onto one axis are plotted in Figure 5. The χ^2 for this fit is found to be 0.98 per degree of freedom. In Figure 5, we note that in the large impact parameter region the contribution of the $b\bar{b}$ component is dominant and it is this region which determines the $b\bar{b}$ fraction.

The fit can be performed for like-sign (LS) and opposite-sign (OS) dimuon events separately. In LS events, there is no contribution from $c\bar{c}$ decays. The prompt LS events are from decays-in-flight and hadronic punchthroughs only since muon pairs from the Drell-Yan process and Υ decay are of opposite-sign. From the fit with the different likelihood functions, we obtain 838 ± 53 LS $b\bar{b}$ events and 1669 ± 88 OS $b\bar{b}$ events where the uncertainties are statistical. These results will be used in Section VII for the mixing analysis.

We also developed an independent method to determine the $b\bar{b}$ fraction in LS dimuon events (see the Appendix). With this method, we find the number of LS $b\bar{b}$ events to be 801 ± 102 , which shows good agreement with the result of the impact parameter fitting.

B. Systematic Uncertainties in the fit

The systematic uncertainty of the fit results from the uncertainties in the shapes of the impact parameter distributions for muons from b decays and prompt muons, and the physics backgrounds such as muons from c decays.

The impact parameter distribution of muons from b decays has some dependence on input parameters to the Monte Carlo simulations. Variation of the average B lifetime by $\pm 6\%$ [7] changes the $b\bar{b}$ fraction by $\pm 5\%$ in the fit. We also take into account the effect of the resolution difference between the Monte Carlo sample and the data. For tracks in a jet, the Monte Carlo resolution ($\sim 19\mu\text{m}$) is found to be different from the data resolution ($\sim 23\mu\text{m}$). We have degraded the Monte Carlo resolution by this difference and used the degraded impact parameter distributions for muons from b decays to determine the central value of the $b\bar{b}$ fraction. The difference in the fraction of $b\bar{b}$ events is found to be 7% and we include this as a systematic uncertainty. The effect of the uncertainty on the fraction of sequential decay muons on the fit has been studied by varying the b fragmentation [22,23] and the branching ratios of semileptonic decays of charm and bottom hadrons [24]. The $b\bar{b}$ fraction changes by $\pm 0.5\%$.

As shown in Figure 2, the impact parameter distribution of jet tracks generally agrees with that of decay muons from π or K . Small variations of the shape of the prompt muon impact parameter distribution negligibly affect the $b\bar{b}$ fraction since it is sensitive to the large impact parameter region where the contribution of prompt muons is negligible. Fitting with impact parameter distributions of various sources of prompt muons such as the Drell-Yan process, bottomonium decays, and decays of π or K , we obtain $\pm 1\%$ systematic uncertainty in the $b\bar{b}$ fraction.

In the H_{sum} term of the likelihood function, we have fixed the relative fraction of $c\bar{c}$ events and events with a muon from a b decay and a prompt muon. By varying the relative fractions of each component in H_{sum} fully from 0% and 100%, we get $\pm 4.7\%$ fractional change in the $b\bar{b}$ fraction. Events with a muon from c decay and a prompt muon may also contribute to the

data. However, the two dimensional impact parameter distribution for these events is very close to that of prompt dimuon events and the inclusion of this component in the likelihood negligibly affects the fit fractions ($\leq 0.5\%$).

The systematic uncertainties of the fit are summarized in Table I. The total systematic uncertainty in the two dimensional fitting method is estimated to be $^{+9.9\%}_{-7.0\%}$.

V. INTEGRAL $b\bar{b}$ CROSS SECTION

We measure the $b\bar{b}$ cross sections with different P_T thresholds for the \bar{b} quark using three exclusive data sets representing three distinct intervals in $P_T(\mu_{\bar{b}})$ for $P_T(\mu_{\bar{b}}) \geq 3$ GeV/c: 3 GeV/c $\leq P_T(\mu_{\bar{b}}) \leq 5$ GeV/c, 5 GeV/c $\leq P_T(\mu_{\bar{b}}) \leq 7$ GeV/c, and $P_T(\mu_{\bar{b}}) \geq 7$ GeV/c. We assign the two muons in an event randomly to the two bottom quarks, thus introducing no kinematical bias. Specifically, we assume that the first and the second muon are decayed from b and \bar{b} respectively even though we do not identify the parent quark explicitly. Each data set is used for a measurement of the integral $b\bar{b}$ cross section with the corresponding P_T constraint for the \bar{b} quark as discussed below Section V.B. The $b\bar{b}$ cross section is given by

$$\sigma(p\bar{p} \rightarrow b\bar{b}X) = \frac{N_{b\bar{b}}}{\int \mathcal{L} dt \cdot Br(b \rightarrow \mu X)^2 \cdot \epsilon_{sel} \cdot A}$$

where $N_{b\bar{b}}$ is the number of $b\bar{b}$ dimuon events and $Br(b \rightarrow \mu X)$ is the branching ratio for the muonic decay of B hadrons (0.103 ± 0.005) [24]. The integrated luminosity $\int \mathcal{L} dt$ used here is 17.4 ± 0.6 pb $^{-1}$. The combined detector and data selection efficiency is ϵ_{sel} and A is the geometrical and kinematical acceptance for $b\bar{b}$ dimuon events.

A. Efficiency

The efficiencies are defined to be multiplicative so that the efficiencies of each data selection requirement are independently measured. In this section, we describe the efficiencies of the individual selection requirements.

The efficiency of the event vertex requirement $|z_0| \leq 30$ cm is measured using a minimum bias data sample which were collected by requiring a $p\bar{p}$ interaction only. The event vertex distribution in the data is parameterized with a Gaussian with a mean of -1.48 ± 0.11 cm and a width of 26.65 ± 0.18 cm [25]. The efficiency is found to be $74.2 \pm 2.1\%$.

The tracking efficiency in the CTC is determined by embedding the CTC hits of Monte Carlo simulated muon tracks in the data sample and then counting the number of reconstructed muon tracks. We measure the efficiency to reconstruct the two muon tracks in $b\bar{b}$ events to be $96 \pm 2\%$.

The muon finding efficiency is measured with dimuon events from J/ψ decays. The dimuon invariant mass spectrum shows a Gaussian resonance peak at the value of the J/ψ mass with a flat background distribution. The number of J/ψ muons is estimated by subtracting the side band region ($2.9 \text{ GeV}/c^2 \leq M_{\mu\mu} \leq 3.0 \text{ GeV}/c^2$, $3.2 \text{ GeV}/c^2 \leq M_{\mu\mu} \leq 3.3 \text{ GeV}/c^2$) from the J/ψ signal region ($3.0 \text{ GeV}/c^2 \leq M_{\mu\mu} \leq 3.2 \text{ GeV}/c^2$). By taking the ratio of the numbers of J/ψ muons before and after the muon matching cuts we measure the muon matching efficiency to be $98.7 \pm 0.2\%$ where the uncertainty represents the statistical error only. In a similar way the muon reconstruction efficiency in the central muon detector (CMU) is found to be $92.1 \pm 2.2\%$. The combined efficiency for the two muons is estimated to be $82.6 \pm 4.4\%$.

We also measure the trigger efficiency using the side-band subtracted J/ψ sample. The measured trigger efficiency at each level is parameterized as a function of the muon P_T and convoluted with the muon P_T distribution obtained from Monte Carlo simulations of b decays in order to measure the overall trigger efficiency. The combined Level 1, Level 2, and Level 3 dimuon trigger efficiencies are listed in Table II for each dimuon data set, where the error comes from the uncertainty in the trigger parameterization.

The track finding efficiency in the SVX is measured by subtracting distributions of like-sign dimuon events from those of opposite-sign events. In the resulting distributions, only the contributions of events from $b\bar{b}$ and $c\bar{c}$ decay, the Drell-Yan process, and Υ decay remain. *Fake* dimuon events (see the Appendix) equally contribute to opposite-sign and like-sign

dimuon candidates and therefore are removed by this subtraction. From a Monte Carlo study based on ISAJET [20] and a detector simulation, this efficiency is shown to be independent of the event topology and represents the efficiency for $b\bar{b}$ dimuon events. This also represents a combined efficiency of the SVX track reconstruction and the SVX geometrical coverage for the two muons in $b\bar{b}$ events with $|z_0| \leq 30$ cm. The dimuon track finding efficiency of the SVX is found to be $66.9 \pm 2.4\%$. The uncertainty results from the statistics of the data sample.

The efficiencies of the impact parameter requirement $d \leq 0.06$ cm are estimated by a Monte Carlo method which consists of ISAJET [20], the CLEO decay package [21], and the full CDF detector simulation. The results are shown in Table II. The errors are from the uncertainty of the average B lifetime [7] used in the Monte Carlo simulation.

The efficiency of the dimuon mass requirement $M_{\mu\mu} \geq 5$ GeV/ c^2 is obtained by a Monte Carlo simulation based on the NLO QCD [5] and the CLEO decay package [21]. The results are given in Table II.

The efficiencies of the trigger, impact parameter cut, and dimuon mass cut exhibit a weak dependence on muon P_T as shown in Table II. On the other hand, the tracking and the muon identification efficiencies are independent of muon P_T in the range of interest.

B. Acceptance

The acceptance is the probability of a muon pair from $b\bar{b}$ decay passing through the region covered by the muon detectors and satisfying the muon P_T requirement. For each muon P_T range, we define the corresponding P_T threshold of bottom quarks (P_T^{min}) as the value such that 90% of muons satisfying the P_T requirement come from b decays with $P_T \geq P_T^{min}$. The values of P_T^{min} are estimated by a Monte Carlo simulation. The Monte Carlo program generates bottom quarks using the input spectra from the next-to-leading order QCD calculation of $b\bar{b}$ production [5]. The generated quarks are fragmented to B hadrons using the Peterson fragmentation function [22], $D(z) = \frac{1}{z} (1-z)^2$. The fragmentation function is defined as $D(z) = \frac{1}{z} \frac{dN}{dz}$, where $z = \frac{P_T}{P_{T,0}}$ is the ratio of the muon transverse momentum to the parent quark transverse momentum, and $\frac{dN}{dz}$ is the differential number of muons per unit transverse momentum.

are decayed by the CLEO Monte Carlo package QQ [21]. For $P_T(\mu_b) \geq 3$ GeV/c, the corresponding P_T^{min} for the b quark is found to be 6.5 GeV/c. The P_T^{min} values for the \bar{b} quark with $P_T(\mu_b) \geq 3$ GeV/c are determined to be 6.5, 8.75, and 12.25 GeV/c respectively, for the $P_T(\mu_b)$ ranges: 3 – 5 GeV/c, 5 – 7 GeV/c, and greater than 7 GeV/c. In addition the rapidity (y) of b and \bar{b} quarks is required to be between -1.0 and 1.0 in order to cover the CMP and CMU fiducial region. The dimuon acceptance is defined as the ratio between the number of $b\bar{b}$ dimuon events satisfying the muon P_T constraints and fiducial requirements and that of $b\bar{b}$ dimuon events with $P_T(b) \geq P_T^{min}(b)$, $P_T(\bar{b}) \geq P_T^{min}(\bar{b})$, and $|y(b)|, |y(\bar{b})| \leq 1$. In the Monte Carlo simulation, muons from semileptonic decays of B hadrons, including sequential decays, are propagated to the CMP detector for the acceptance calculation. The results are shown in Table III. The systematic uncertainty of the acceptance comes from the uncertainty in our model for b quark fragmentation and the fraction of sequential decay muons. Changing the Peterson fragmentation parameter [23] by ± 0.002 results in a $\pm 9\%$ uncertainty in the acceptance. The effect of the fraction of sequential decay muons on the acceptance is studied by varying the relative branching ratio of bottom and charm semileptonic decays [24] and is estimated to be $\pm 4\%$. In total, the systematic uncertainty of the acceptance is found to be $\pm 9.8\%$.

C. $N_{b\bar{b}}$

In order to measure $N_{b\bar{b}}$, we use the two dimensional impact parameter fitting method as discussed in Section IV. In each data set, we perform the fit with the corresponding template histograms. The fit results are listed in Table III.

D. Result

Our measurements of the $b\bar{b}$ cross section for $P_T(b) \geq P_T^{min}(b)$, $P_T(\bar{b}) \geq P_T^{min}(\bar{b})$, and $|y_b|, |y_{\bar{b}}| \leq 1$ are shown in Table III. The systematic errors dominate and are correlated for the different measurements. The NLO QCD calculation of $b\bar{b}$ production is given by

Reference [5]. In the calculation, we use the MRSD0 structure functions [26], the renormalization scale $\mu = \mu_0 \equiv \sqrt{m_b^2 + (P_T(b)^2 + P_T(\bar{b})^2)/2}$, and $\Lambda_5 = 140$ MeV with $m_b = 4.75$ GeV/ c^2 . Figure 6 shows the comparison between the measured $b\bar{b}$ cross sections and the NLO QCD prediction. The uncertainty of the prediction is obtained by varying the QCD parameters within the range of acceptable values [27]: $\mu = \mu_0/2 - 2\mu_0$, $\Lambda_5 = 100 - 300$ MeV, and $m_b = 4.5 - 5$ GeV/ c^2 . The measured $b\bar{b}$ cross section is consistently higher than the prediction of NLO QCD as has been observed in other measurements [1–4]. The shape of the $b\bar{b}$ cross section agrees with the theoretical prediction.

VI. $\mu - \mu$ CORRELATIONS

We have also investigated correlations between the two muons from $b\bar{b}$ decays. The geometrical correlation is studied by examining the distribution of the opening angle in the transverse plane, $\delta\phi_{\mu\mu}$, between the muons with $P_T \geq 3$ GeV/ c . The two-dimensional impact parameter fit is independently performed in each $\delta\phi$ bin to obtain the number of $b\bar{b}$ events. The dimuon cross section in each bin is listed in Table IV. In order to study kinematic correlations, the $P_T(\mu_{\bar{b}})$ distribution with $P_T(\mu_b) \geq 3$ GeV/ c is obtained using the impact parameter fitting technique for each P_T bin. The results are shown in Table IV and the errors include both statistical and systematic uncertainties of the fit.

We compare the observed correlations with a Monte Carlo model based on the NLO QCD calculation [5] which gives the exact $b\bar{b}$ cross section at $O(\alpha_s^3)$. The model predicts the b quark momentum distribution, the momentum of the B hadron from the momentum of the b quark using the Peterson fragmentation function, and the muon momentum from the momentum of the B hadron using the momentum distributions of muons in the rest frame of B hadrons [28]. We obtain the predicted dimuon cross section by weighting the Monte Carlo events with the branching ratio of $B \rightarrow \mu X$ decay [24] and the efficiencies of the CDF detector and data selection. Figures 7 and 8 show a comparison between the measurements and the predictions of the model. The QCD calculation uses the MRSD0 structure functions

[26] and the same QCD parameters as used in Section V.D. The uncertainty of the predictions includes the systematic uncertainties of the weights and the uncertainty in the fragmentation [23]. Figure 9 shows that the shape of the P_T distribution for μ_b agrees well with the prediction although the values of the dimuon cross section are significantly higher. The $\delta\phi$ distribution from the data also shows reasonable agreement with the model prediction in addition to a higher normalization as shown in Figure 9.

VII. AVERAGE $B^0\bar{B}^0$ MIXING PARAMETER

The average $B^0\bar{B}^0$ mixing parameter, $\bar{\chi}$, is defined as

$$\bar{\chi} = \frac{\Gamma(B^0 \rightarrow \bar{B}^0 \rightarrow \mu^- X)}{\Gamma(B \rightarrow \mu^\pm X)}$$

where the numerator includes B_d^0 and B_s^0 mesons and the denominator includes all the B hadrons. In the absence of mixing, the double semileptonic decay of a $B\bar{B}$ pair results in an opposite-sign muon pair. A $B\bar{B}$ pair where one of the mesons undergoes mixing ($B^0 \rightarrow \bar{B}^0$ or vice versa) produces a like-sign muon pair. The $B^0\bar{B}^0$ mixing can be studied by measuring the ratio, R , of the number of $b\bar{b}$ like-sign events to that of $b\bar{b}$ opposite-sign events.

The sequential decays ($b \rightarrow cX \rightarrow \mu Y$) also contribute to R . The fraction of muons from sequential decays, f_{seq} , is found to be 0.123 ± 0.015 from a Monte Carlo simulation based on the full next-to-leading-order QCD calculation. The uncertainty of the fraction of sequential muons ($\pm 12\%$) comes from the uncertainty of the relative branching ratio of bottom and charm semileptonic decays ($\pm 11\%$) [24] and the uncertainty of the relative muon acceptance ($\pm 6\%$).

In $b\bar{b}$ dimuon events, the ratio, R , of the number of like-sign events, N_{LS} , to that of opposite-sign events, N_{OS} , is related to the time and flavor averaged $B\bar{B}$ mixing parameter $\bar{\chi}$ in the following way.

$$R = \frac{N_{LS}}{N_{OS}} = \frac{2f_{seq}(\bar{\chi}^2 + (1 - \bar{\chi})^2) + 2\bar{\chi}(1 - \bar{\chi})(1 + f_{seq}^2)}{(\bar{\chi}^2 + (1 - \bar{\chi})^2)(1 + f_{seq}^2) + 4f_{seq}\bar{\chi}(1 - \bar{\chi})}$$

where f_{seq} is the fraction of muons from sequential decays.

The two dimensional impact parameter fitting method is used to determine the number of $b\bar{b}$ events in the like-sign and opposite-sign data samples. The log likelihood functions and the fit results for LS and OS dimuon events are described in Section IV where we obtain 838 ± 53 like-sign (LS) and 1669 ± 88 opposite-sign (OS) events. In opposite-sign (OS) events, the inclusion of $c\bar{c}$ events results in $\pm 4.7\%$ uncertainty in the fit fraction for $b\bar{b}$ events as described in Section IV. Other sources of systematic uncertainties cancel out in the ratio R which is measured to be $0.502 \pm 0.041(stat) \pm 0.024(sys)$. From the observed value of R , the $B\bar{B}$ mixing parameter $\bar{\chi}$ is measured to be $0.131 \pm 0.020(stat) \pm 0.016(sys)$, consistent with previous measurements [29–33].

VIII. CP VIOLATING ASYMMETRY

CP violation in the B system gives different mixing probabilities for B^0 and \bar{B}^0 mesons [34]. In dimuon events from $B\bar{B}$ decay, the effect of CP violation appears as an asymmetry between $\mu^+\mu^+$ and $\mu^-\mu^-$ events where one of the neutral B mesons has mixed. By measuring the charge asymmetry we can determine the real part of the CP violating parameters ϵ_d and ϵ_s [34] where the subscript of ϵ represents the light quark flavor of the corresponding neutral B meson.

We measure the number of $\mu^+\mu^+$ events and $\mu^-\mu^-$ events from $b\bar{b}$ decays using the two dimensional impact parameter fitting technique. From the fit, we obtain 428 ± 37 $\mu^+\mu^+$ events and 410 ± 37 $\mu^-\mu^-$ events. The observed dimuon charge asymmetry, A_{obs} , can be defined as $\frac{N_{++} - N_{--}}{N_{++} + N_{--}}$ and is measured to be $(2.2 \pm 6.3) \times 10^{-2}$.

In order to extract the dimuon charge symmetry due to CP violation (A_{cp}) from the value of A_{obs} , we must account for any experimental bias in the measured asymmetry in the number of $\mu^+\mu^+$ and $\mu^-\mu^-$ events. This experimental bias may result from the track reconstruction or the dimuon trigger. The charge bias of track reconstruction in CDF is measured using minimum bias data. By applying the same data selection criteria except

for muon identification requirements, we determine the charge asymmetry for single tracks, $\frac{N_+ - N_-}{N_+ + N_-}$. The dimuon charge asymmetry is 2 times the single track charge asymmetry, since there are two muon tracks in an event, and is found to be $(0.7 \pm 2.5) \times 10^{-2}$ where the error comes from statistics in the minimum bias data. The charge bias of the dimuon trigger is studied using the side-band subtracted J/ψ sample as described in Section V.A. By parameterizing the trigger at each level as a function of muon P_T and convoluting the P_T distribution of muons from b decays for μ^+ and μ^- , we obtain $(-0.9 \pm 2.1) \times 10^{-2}$ for the asymmetry of the dimuon trigger.

The charge asymmetry due to CP violation, A_{cp} , is estimated by subtracting the above bias from the measured asymmetry A_{obs}

$$A_{cp} = (2.4 \pm 6.3(stat) \pm 3.3(sys)) \times 10^{-2}$$

A muon from sequential B decay will also result in a like-sign muon pair. The contribution of sequential muons to A_{cp} must be taken into account and from the phenomenology of CP violation in the B system [34], A_{cp} can be expressed as

$$A_{cp} = \frac{8(1 - \bar{\chi})}{D} \left\{ f_d \chi_d \frac{Re(\epsilon_d)}{1 + |\epsilon_d|^2} + f_s \chi_s \frac{Re(\epsilon_s)}{1 + |\epsilon_s|^2} \right\}$$

$$D = 2\bar{\chi}(1 - \bar{\chi})(1 + f_{seq}^2) + 2f_{seq} \{ \bar{\chi}^2 + (1 - \bar{\chi})^2 \}$$

where f_d and f_s are the fractions of B_d^0 and B_s^0 and χ_d and χ_s are the corresponding mixing parameters. The dilution factor D includes the effect of the mixing of the other B meson and sequential decays. The fraction of sequential muons (f_{seq}) is found to be 0.123 ± 0.015 from the Monte Carlo calculation as discussed in Section VII. Using the world average value of $\bar{\chi}$ (0.133 ± 0.011) [11] we obtain one constraint for four quantities - $Re(\epsilon_d)$, $Im(\epsilon_d)$, $Re(\epsilon_s)$, and $Im(\epsilon_s)$ as follows.

$$f_d \chi_d \frac{Re(\epsilon_d)}{1 + |\epsilon_d|^2} + f_s \chi_s \frac{Re(\epsilon_s)}{1 + |\epsilon_s|^2} = (1.5 \pm 3.8(stat) \pm 2.0(sys)) \times 10^{-3}$$

Using the values of f_d (0.391), f_s (0.117), χ_d (0.156), and χ_s (0.62) from the Particle Data Group [11], one can plot the region constrained by the above result in the $\frac{Re(\epsilon_d)}{1 + |\epsilon_d|^2} - \frac{Re(\epsilon_s)}{1 + |\epsilon_s|^2}$ space

along with the result on $\frac{Re(\epsilon_d)}{1+|\epsilon_d|^2}$ from the CLEO experiment [35] in Figure 10. It shows that the result of this analysis is sensitive to a few $\times 10^{-2}$ at 1σ level for $Re(\epsilon_{d,s})$ and consistent with the prediction of the Standard Model for CP violation in the B system ($\epsilon_{d,s} \sim 10^{-3}$) [36].

IX. CONCLUSIONS

We have presented results on $b\bar{b}$ correlations, the average $B^0\bar{B}^0$ mixing parameter $\bar{\chi}$, and the CP violating parameter ϵ_B using dimuon events from $b\bar{b}$ decay. For the studies of $b\bar{b}$ correlations, we have measured the $b\bar{b}$ cross section as a function of $P_T(\bar{b})$, the opening angle distribution between the two muons from $b\bar{b}$ decays, and the muon P_T distribution with a P_T constraint on the other muon in $b\bar{b}$ events. These results show consistently higher values than the predictions of the NLO QCD theory. A qualitative picture of $b\bar{b}$ production has been obtained by the studies of $\mu-\mu$ correlations. The shape of the muon P_T distribution agrees well with the theory. The shape of the opening angle between the two muons from $b\bar{b}$ decays is also found to be consistent with the theory within the uncertainties.

With the same technique used in the $b\bar{b}$ correlation studies, the $B\bar{B}$ mixing parameter is measured to be $0.131 \pm 0.020(stat) \pm 0.016(sys)$ consistent with the previous measurements [29–33]. We have also searched for CP violation in the B system by measuring the charge asymmetry in $\mu^+\mu^+$ and $\mu^-\mu^-$ events. The result is consistent with the Standard model prediction [36].

X. ACKNOWLEDGEMENTS

We thank the Fermilab staff and the technical staffs of the participating institutions for their vital contributions. This work was supported by the U.S. Department of Energy and National Science Foundation; the Italian Istituto Nazionale di Fisica Nucleare; the Ministry of Education, Science and Culture of Japan; the Natural Sciences and Engineering Research

Council of Canada; the National Science Council of the Republic of China; the A. P. Sloan Foundation; and the Alexander von Humboldt-Stiftung.

XI. APPENDIX

We present another independent method to obtain the $b\bar{b}$ fraction in the dimuon data. It gives the $b\bar{b}$ fraction in like-sign (LS) dimuon events only and serves as a check of the result of the impact parameter fitting method.

Reconstructed muons in the CMU detector can be divided into the two types of muons – *real* muons and *fakes*. *Real* muons are defined here as muons from b or c semileptonic decays, the Drell-Yan process, and Υ decay. *Fakes* are defined here to be not *real* and include muons from π or K decays and hadronic punchthroughs misidentified as muons. Reconstructed muons in the CMU detector pass through an additional 3 absorption lengths of material (iron) and may or may not make muon segments in the CMP detector. The probability of a CMU muon making a segment in the CMP chamber, called the CMP efficiency, is different for *real* muons and *fakes*. For *real* muons, it is expected to be close to 100% due to the small absorption rate of muons for $P_T \geq 3 \text{ GeV}/c$. For *fakes*, most of the hadronic punchthroughs are absorbed inside the iron between the CMU and CMP detector but most of the decay muons from π or K pass through the material to the CMP detector. The CMP efficiency for *fakes* is then expected to be very different from that for *real* muons, depending on the relative fractions of decay muons and hadronic punchthroughs. The principle of this method is to fully exploit the difference of the CMP efficiencies between *real* muons and *fakes* in order to obtain the fraction of *real* dimuons in like-sign(LS) dimuon events. In like-sign events, only $b\bar{b}$ pairs can generate *real* dimuon events via sequential B decay ($b \rightarrow cX \rightarrow \mu Y$) or $B^0\bar{B}^0$ mixing and we directly obtain the $b\bar{b}$ fraction from the fraction of *real* dimuon events.

The data sample for the CMP efficiency method is different from the standard data used in the impact parameter fitting technique. We require neither a muon segment in the CMP nor a track in the SVX and only $\mu^-\mu^-$ events are used. In addition, a muon is required to

be in the fiducial region of the CMP in order to apply the CMP efficiency method.

We count the number of dimuon events with both muons having a muon segment in the CMP, N_2 , only one of the muons having a muon segment in the CMP, N_1 , and neither of the muons having a muon segment in the CMP, N_0 . With the CMP efficiency, ϵ_μ , for *real* muons and the CMP efficiency, ϵ_f , for *fakes*, we construct three equations for the above three different types of dimuon events:

$$N_0 = (1 - \epsilon_\mu)^2 M + (1 - \epsilon_\mu)(1 - \epsilon_f)F_1 + (1 - \epsilon_f)^2 F_2$$

$$N_1 = 2\epsilon_\mu(1 - \epsilon_\mu)M + \{\epsilon_\mu(1 - \epsilon_f) + \epsilon_f(1 - \epsilon_\mu)\}F_1 + 2\epsilon_f(1 - \epsilon_f)F_2$$

$$N_2 = \epsilon_\mu^2 M + \epsilon_\mu \epsilon_f F_1 + \epsilon_f^2 F_2$$

where the number of *real* dimuon events (or $b\bar{b}$ dimuon events) is represented by M and the number of *fake* dimuon events by F . The subscript of F denotes the number of *fakes* in an event. From the data we have a total of 3423 $\mu^-\mu^-$ events consisting of 592 events for N_0 , 1430 events for N_1 , and 1401 events for N_2 .

The CMP efficiency for *real* muons, ϵ_μ , is measured to be 0.94 ± 0.01 using dimuon events from $J/\psi \rightarrow \mu^+\mu^-$ decay. The CMP efficiency for *fakes*, ϵ_f , is determined from the study of $K_S^0 \rightarrow \pi^+\pi^-$ decays where the negatively charged pion generates a muon signal in the muon detector via decay $\pi^- \rightarrow \mu^- \bar{\nu}_\mu$ or punchthrough. We reconstruct K_S^0 events with a negatively charged muon signal and a positively charged track and measure ϵ_f to be 0.49 ± 0.04 using a muon leg of the K_S^0 event. From a Monte Carlo study including the full detector simulation, the effect of the *fakes* from kaons on ϵ_f is found to be negligible. In $\mu^+\mu^+$ events, we can not determine ϵ_f in a similar way due to the different punchthrough rates for a pion and a kaon [18]. Using the measured CMP efficiencies, we solve the equations and obtain 736 ± 89 events for M where the uncertainty represents both statistical uncertainty and systematic uncertainty of the measured CMP efficiencies.

For a comparison with the result of the two-dimensional fitting method, we convert the above number to the number of $b\bar{b}$ events in the standard like-sign dimuon data where

a muon is required to have a muon segment in the CMP and a track in the SVX. From the assumption of charge symmetry for $b\bar{b}$ dimuon events, we can assume $M^{--} = M^{++}$. Therefore the number of $b\bar{b}$ events in the standard like-sign dimuon data, $N_{b\bar{b}}^{LS}$, can be calculated using the following relation.

$$N_{b\bar{b}}^{LS} = 2 \cdot M \cdot \epsilon_{\mu}^2 \cdot \epsilon_{svx} \cdot \epsilon_{imp}$$

where the CMP efficiency ϵ_{μ} is found to be 0.94 ± 0.01 , track finding efficiency in the SVX for $b\bar{b}$ dimuons, ϵ_{svx} , is found to be 0.669 ± 0.024 (from Table II), and the impact parameter cut efficiency for $b\bar{b}$ dimuons, ϵ_{imp} , is found to be 0.921 ± 0.006 from a Monte Carlo simulation. With these efficiencies, we obtain 801 ± 102 $b\bar{b}$ events in the standard like-sign dimuon events, which is in good agreement with the result of the impact parameter fit (838 ± 53 events from Section IV.A). The result independently confirms the validity of the two dimensional impact parameter fitting method.

REFERENCES

- [1] F. Abe *et al.*, CDF Collaboration, Phys. Rev. Lett. **71**, 2396 (1993).
- [2] F. Abe *et al.*, CDF Collaboration, Phys. Rev. Lett. **75**, 1451 (1995).
- [3] S. Abachi *et al.*, D0 Collaboration, Phys. Rev. Lett. **74**, 3548 (1995).
- [4] F. Abe *et al.*, CDF Collaboration, Phys. Rev. D **53**, 1051 (1996).
- [5] M. Mangano, P. Nason, and G. Ridolfi, Nucl. Phys. B **373**, 295 (1992).
- [6] M. Kobayashi and T. Maskawa, Prog. Theor. Phys. **49**, 652 (1973).
- [7] F. Abe *et al.*, CDF Collaboration, Phys. Rev. Lett. **71**, 3421 (1993). In this paper, the average B lifetime is measured to be 1.46 ± 0.085 picosecond. We use this value for the analysis.
- [8] F. Abe *et al.*, CDF Collaboration, Phys. Rev. Lett. **72**, 3456 (1994).
- [9] P. Abreu *et al.*, DELPHI Collaboration, Z. Phys. C **57**, 181 (1993).
- [10] D. Buskulic *et al.*, ALPEH Collaboration, Phys. Lett. B **314**, 459 (1993).
- [11] Particle Data Group, Review of Particle Properties, Phys. Rev. D **50** (1994).
- [12] F. Abe *et al.*, Nucl. Instrum. Methods A **271**, 387 (1988).
- [13] D. Amidei *et al.*, Nucl. Instrum. Methods A **350**, 73 (1994).
- [14] F. Bedeschi *et al.*, Nucl. Instrum. Methods A **268**, 51 (1988).
- [15] G. Ascoli *et al.*, Nucl. Instrum. Methods A **268**, 33 (1988).
- [16] J. Chapman *et al.*, to be submitted to Nucl. Instrum. Methods.
- [17] G. W. Foster *et al.*, Nucl. Instrum. Methods A **269**, 93 (1988).
- [18] I. Yu, Ph.D. Thesis, Yale University, May 1996 (unpublished).

- [19] F. Abe *et al.*, Phys. Rev. D **50**, 2966 (1994).
- [20] F. Paige and S. D. Protopopescu, BNL Report No. 38034, 1986 (unpublished). We used version 6.36.
- [21] P. Avery, K. Read, and G. Trahern, Cornell Internal Note CSN-212, March 25, 1985 (unpublished). We used QQ version 9.00.
- [22] C. Peterson *et al.*, Phys. Rev. D **27**, 105 (1983).
- [23] J. Chrin, Z. Phys. C **36**, 165 (1987). The fragmentation parameter ϵ is assumed to be 0.006 ± 0.002 in this analysis.
- [24] In this analysis, we use the branching ratios $Br(b \rightarrow \mu X) = 0.103 \pm 0.005$ and $Br(b \rightarrow cX \rightarrow \mu Y) = 0.102 \pm 0.010$ based on the branching ratios for the individual hadrons from the Particle Data Group.
- [25] W. Badgett, Ph. D. thesis, University of Michigan, 1994 (unpublished).
- [26] A. D. Martin, R. G. Roberts, and W. J. Stirling, RAL-92-021(1992).
- [27] M. Mangano, CERN-TH-95-191, Proceedings of the 6th International Symposium on Heavy Flavor Physics, Pisa, Italy.
- [28] We use the model to minimize the statistical jitter at the lepton level arising from the divergences inherent in the calculation [5]. The details of the model are described in Reference [18].
- [29] F. Abe *et al.*, CDF Collaboration, Phys. Rev. Lett. **67**, 3351 (1991).
- [30] C. Albajar *et al.*, UA1 Collaboration, Phys. Lett. B **262**, 171 (1991).
- [31] P. Acton *et al.*, OPAL Collaboration, Phys. Lett. B **276**, 379 (1992).
- [32] B. Adeva *et al.*, L3 Collaboration, Phys. Lett. B **288**, 395 (1992).
- [33] P. Abreu *et al.*, DELPHI Collaboration, Phys. Lett. B **301**, 145 (1993).

- [34] I. I. Bigi *et al.*, in CP Violation ed. C. Jarlskog, World Scientific, Singapore (1989).
- [35] J. Bartelt *et al.*, CLEO Collaboration, Phys. Rev. Lett. **71**, 1680 (1993).
- [36] T. Altomari, T. L. Wolfenstein, and J. D. Bjorken, Phys. Rev. D **37**, 1860 (1988).

FIGURES

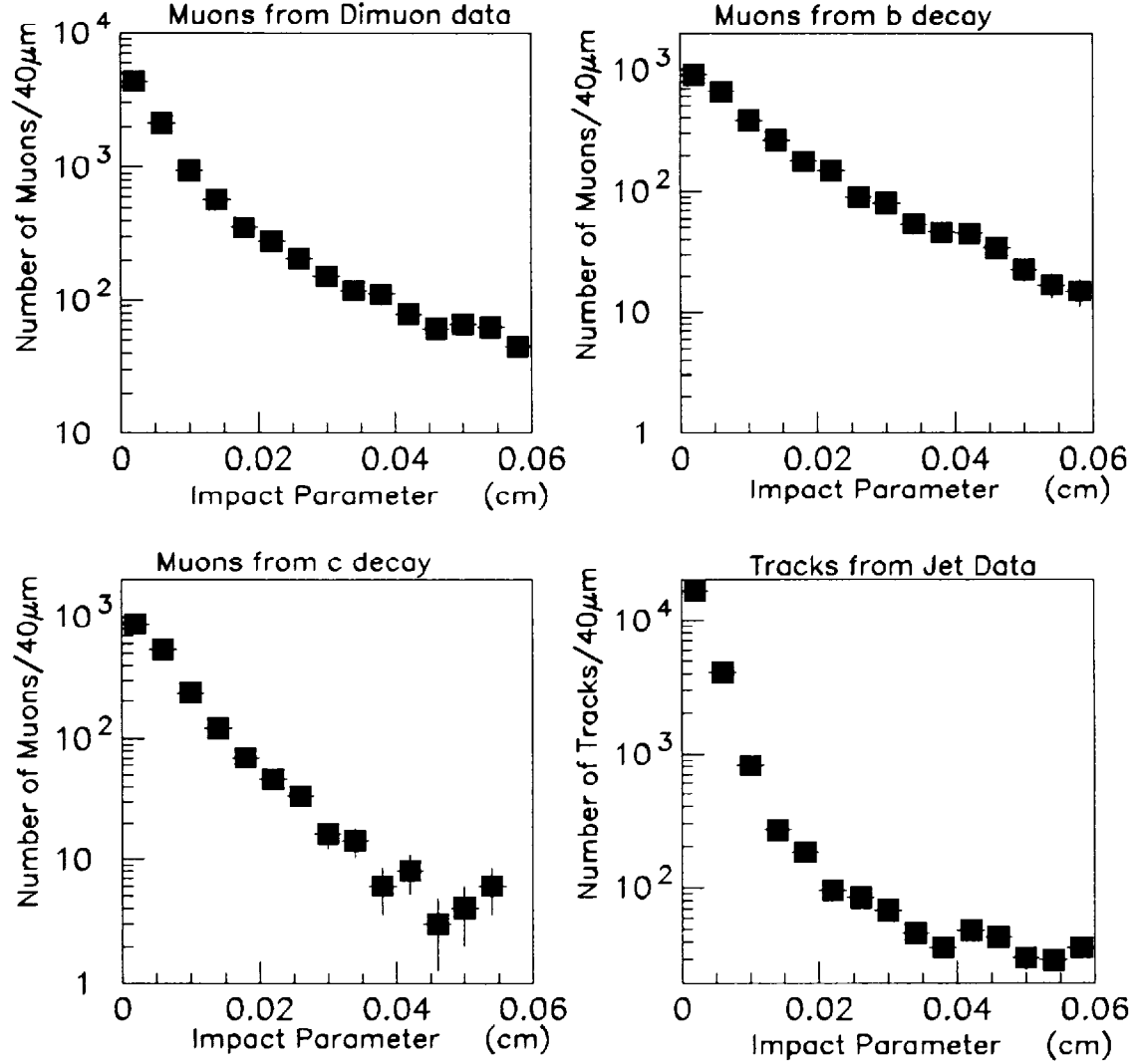


FIG. 1. Impact parameter distributions of muons of various sources with $P_T \geq 3 \text{ GeV}/c$. The distributions for muons from b and c decays are generated from the Monte Carlo simulation with the average $c\tau_B = 438 \mu\text{m}$ and $c\tau_D = 183 \mu\text{m}$.

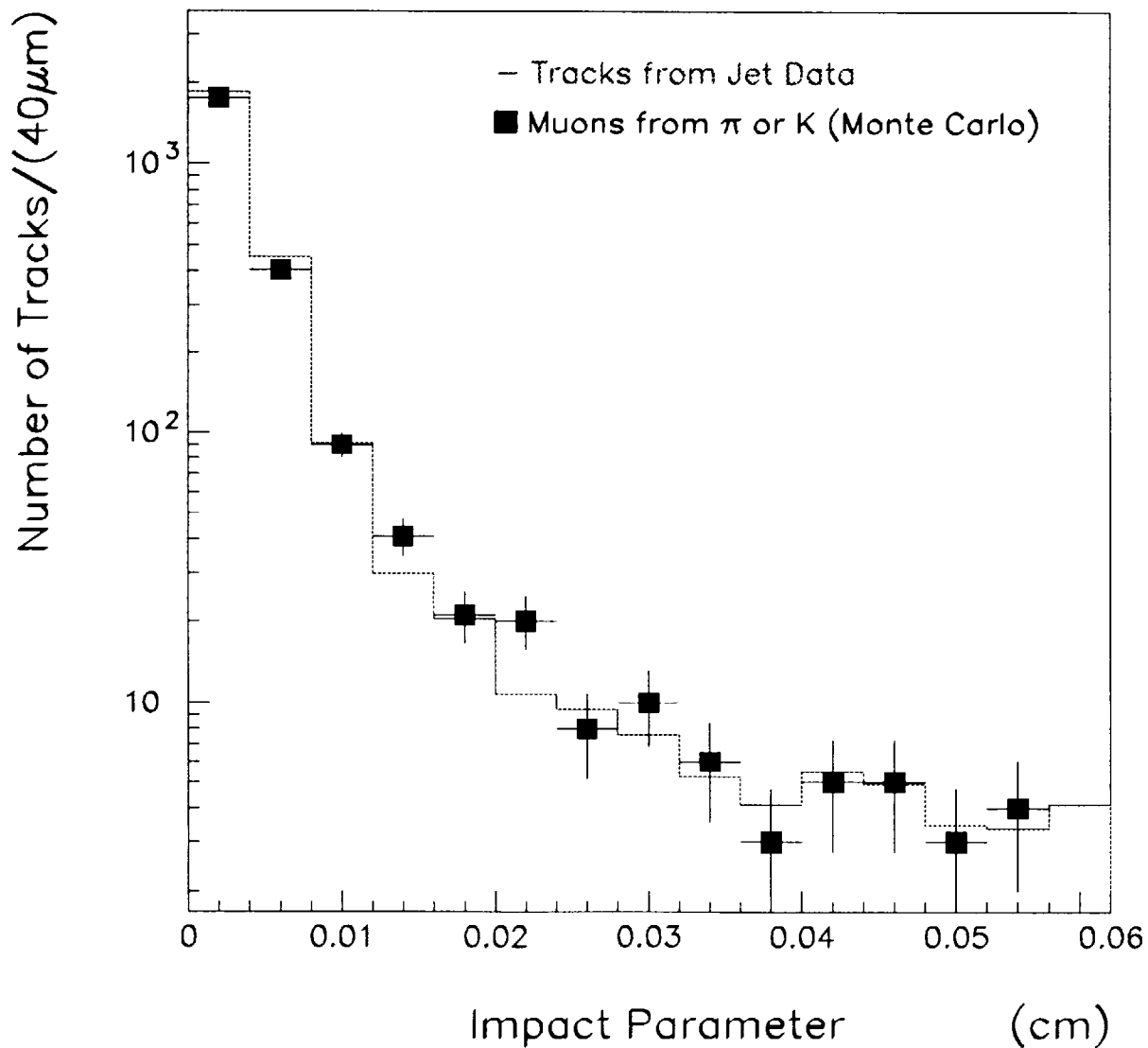


FIG. 2. Comparison between an impact parameter distribution of jet tracks and that of decay muons from π or K with $P_T \geq 3$ GeV/c. A Monte Carlo simulation is used to obtain the impact parameter distribution of decay muons. The ratio of K to π is set to be 1/3 in the Monte Carlo simulation.

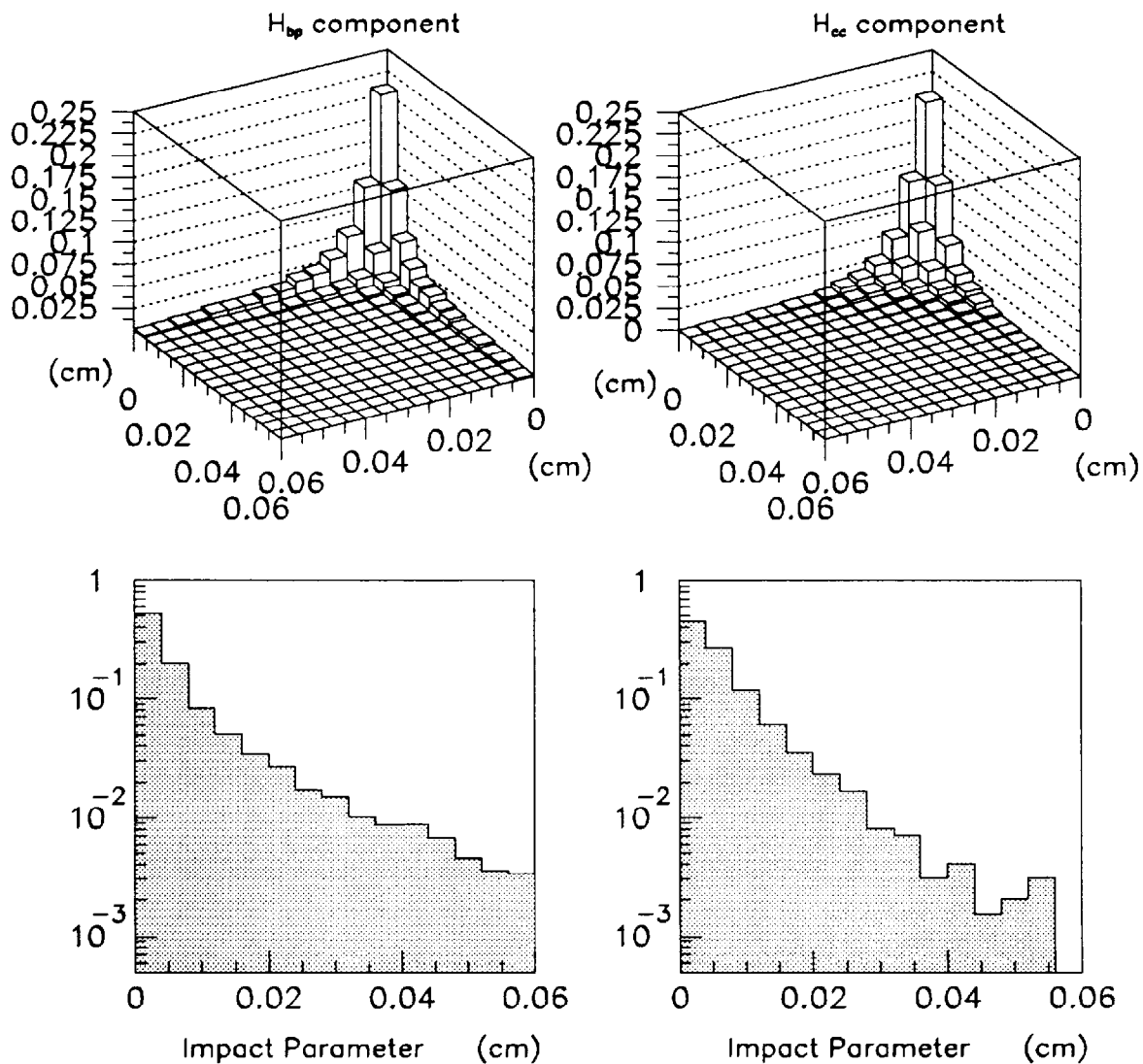


FIG. 3. The upper two plots are two dimensional impact parameter distributions for each component. The lower plots are projections of these histograms onto one of the two axes. The $c\bar{c}$ component is represented by H_{cc} and the component from events with a muon from a b decay and a prompt muon by H_{bp} .

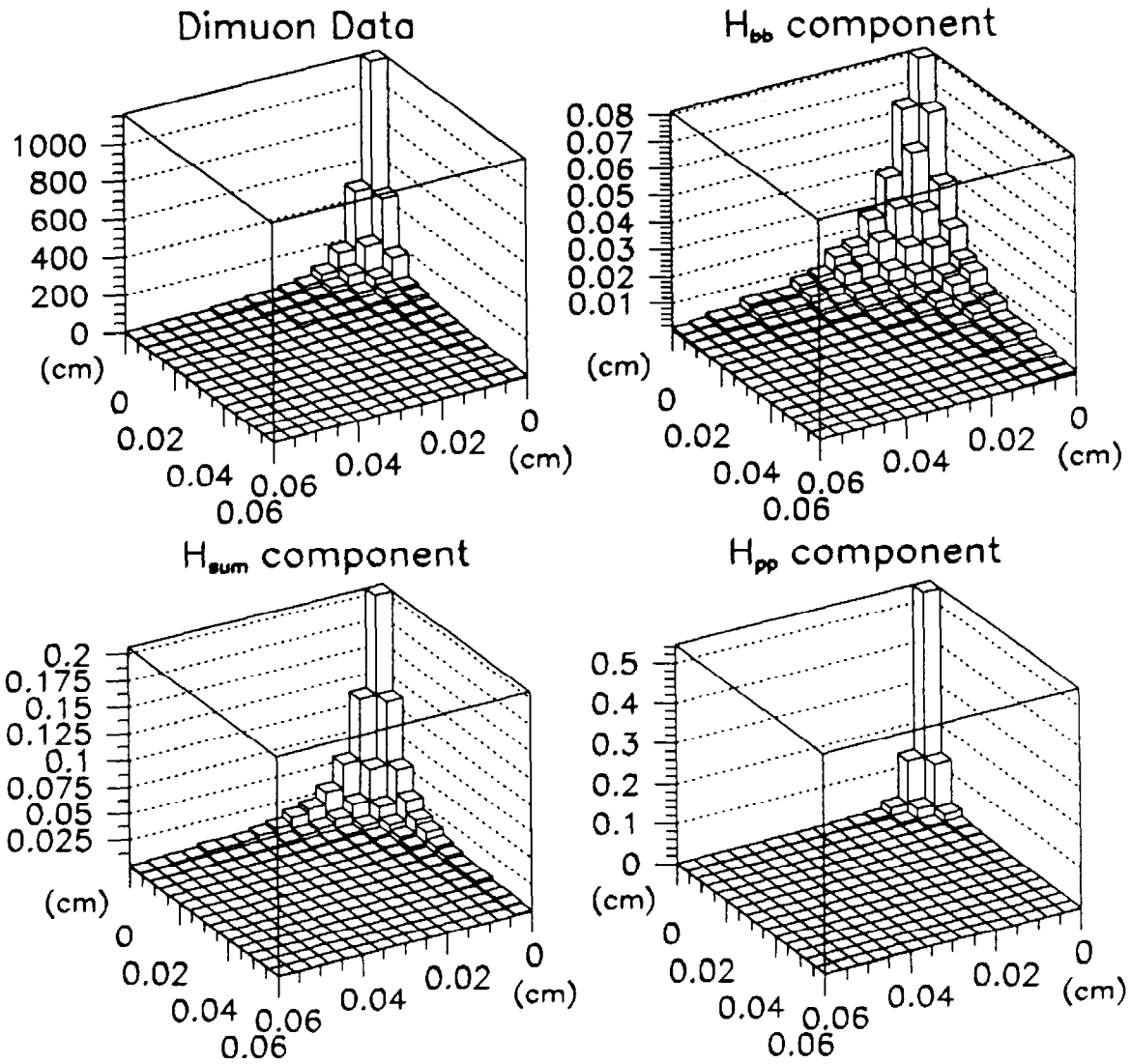


FIG. 4. Two dimensional impact parameter distributions from data and each component. The template histograms for each component are normalized to 1.

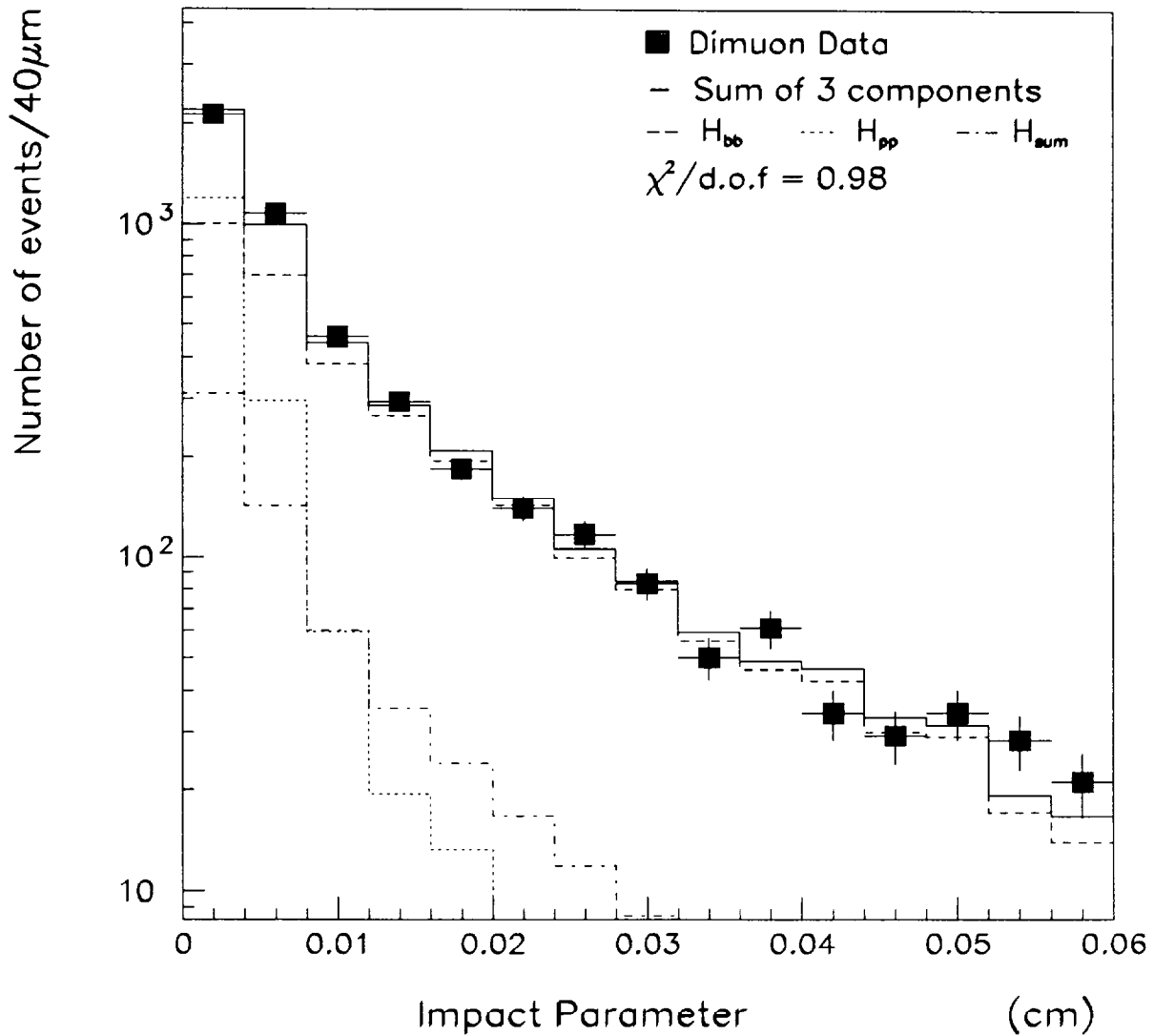


FIG. 5. Comparison between the projection of the data distribution and a sum of the 3 components. The contribution of $b\bar{b}$ events is denoted by H_{bb} , that of prompt dimuon events by H_{pp} , and that of $c\bar{c}$ events and events with a muon from a b decay and a prompt muon by H_{sum} .

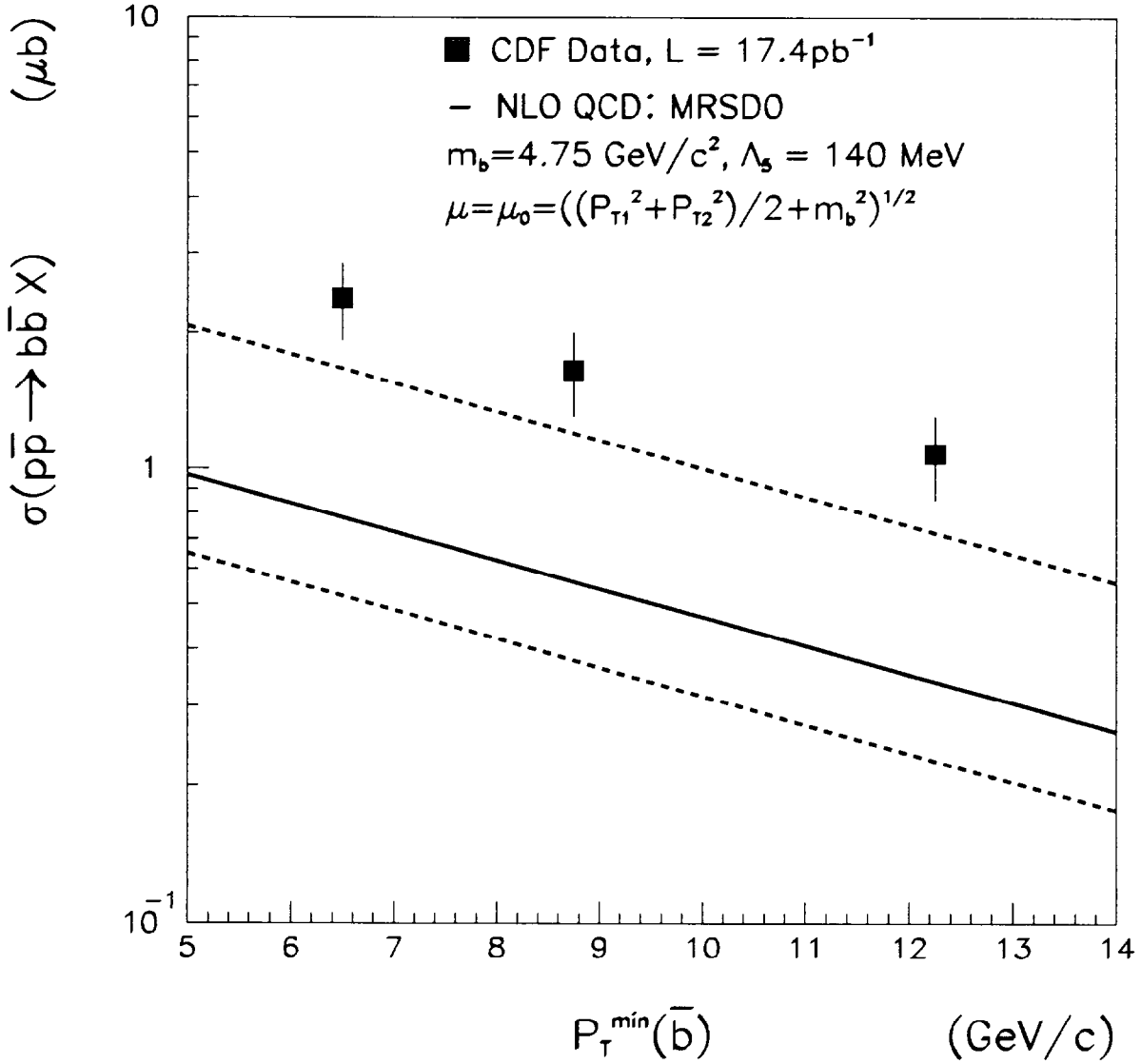


FIG. 6. Integral $b\bar{b}$ cross section with $P_T(b) \geq 6.5\text{ GeV}/c$, $|y_b|, |y_{\bar{b}}| \leq 1$, and $P_T(\bar{b}) \geq P_T^{\min}(\bar{b})$. The uncertainty of the prediction (dashed line) comes from the variation of QCD parameters: $m_b = 4.5 - 5\text{ GeV}/c^2$, $\mu = \mu_0/2 - 2\mu_0$, $\Lambda_5 = 100 - 300\text{ MeV}$.

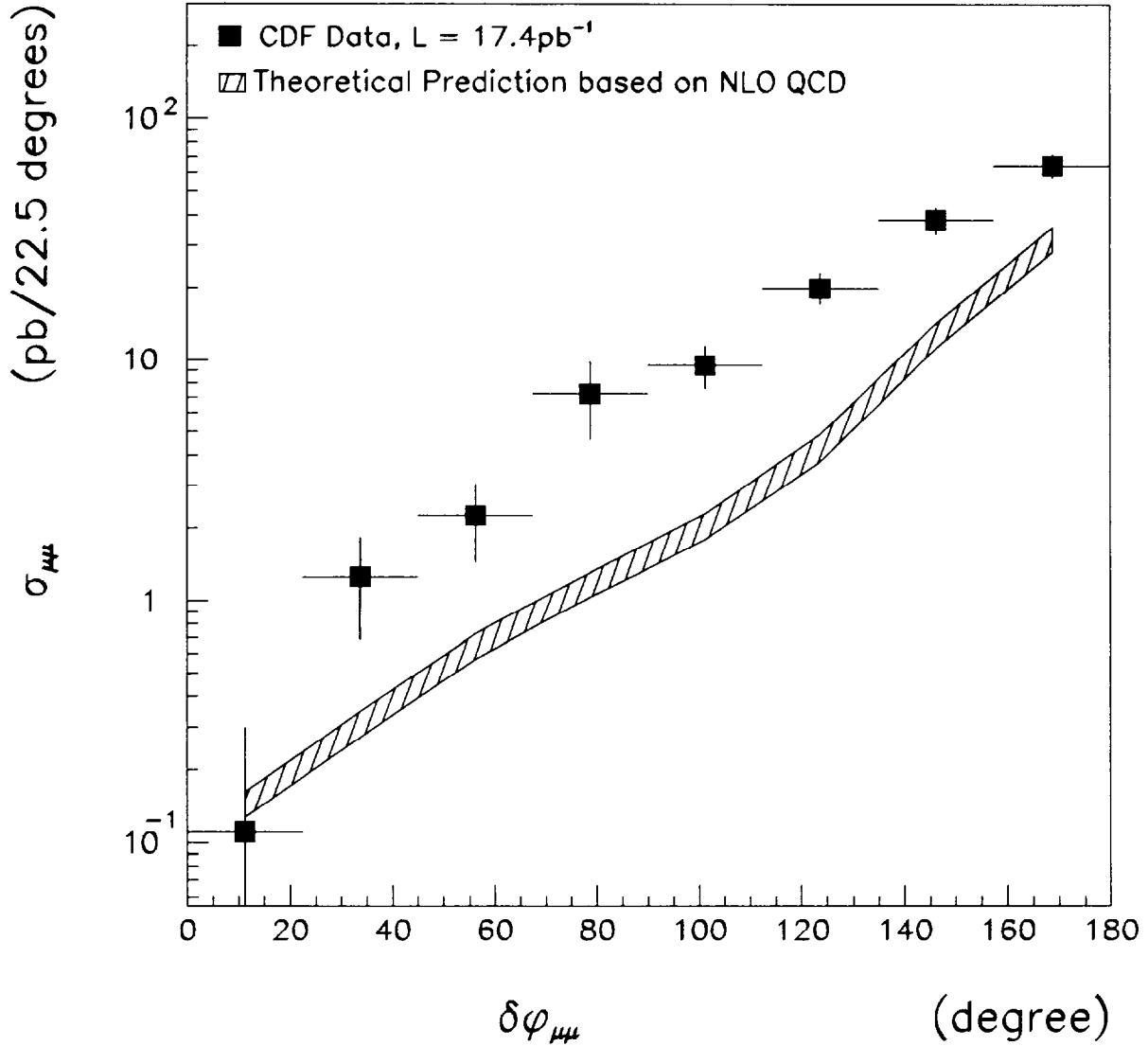


FIG. 7. Opening angle distribution between the two muons from $b\bar{b}$ decays. The data points have a common systematic uncertainty of the fit ($^{+9.9}_{-7.0}\%$) and of the luminosity ($\pm 3.6\%$). The uncertainties of theoretical prediction are from efficiencies, branching ratio of $B \rightarrow \mu X$, and the b quark fragmentation.

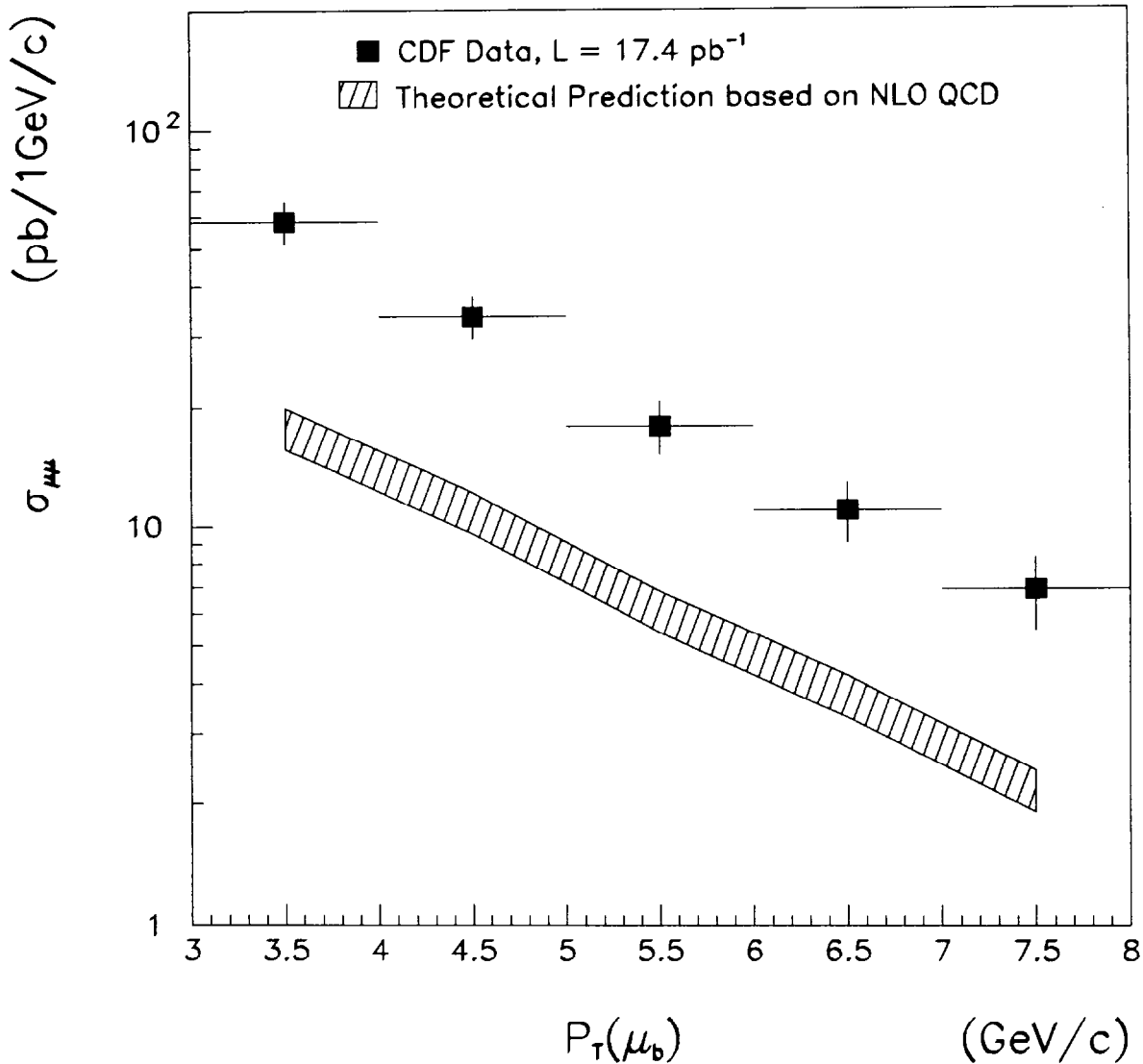


FIG. 8. $P_T(\mu_{\bar{b}})$ distribution for $P_T(\mu_b) \geq 3$ GeV/c. The data points have a common systematic uncertainty of the fit ($^{+9.9}_{-7.0}\%$) and of the luminosity ($\pm 3.6\%$). The uncertainties of theoretical prediction are from efficiencies, branching ratio of $B \rightarrow \mu X$, and the b quark fragmentation.

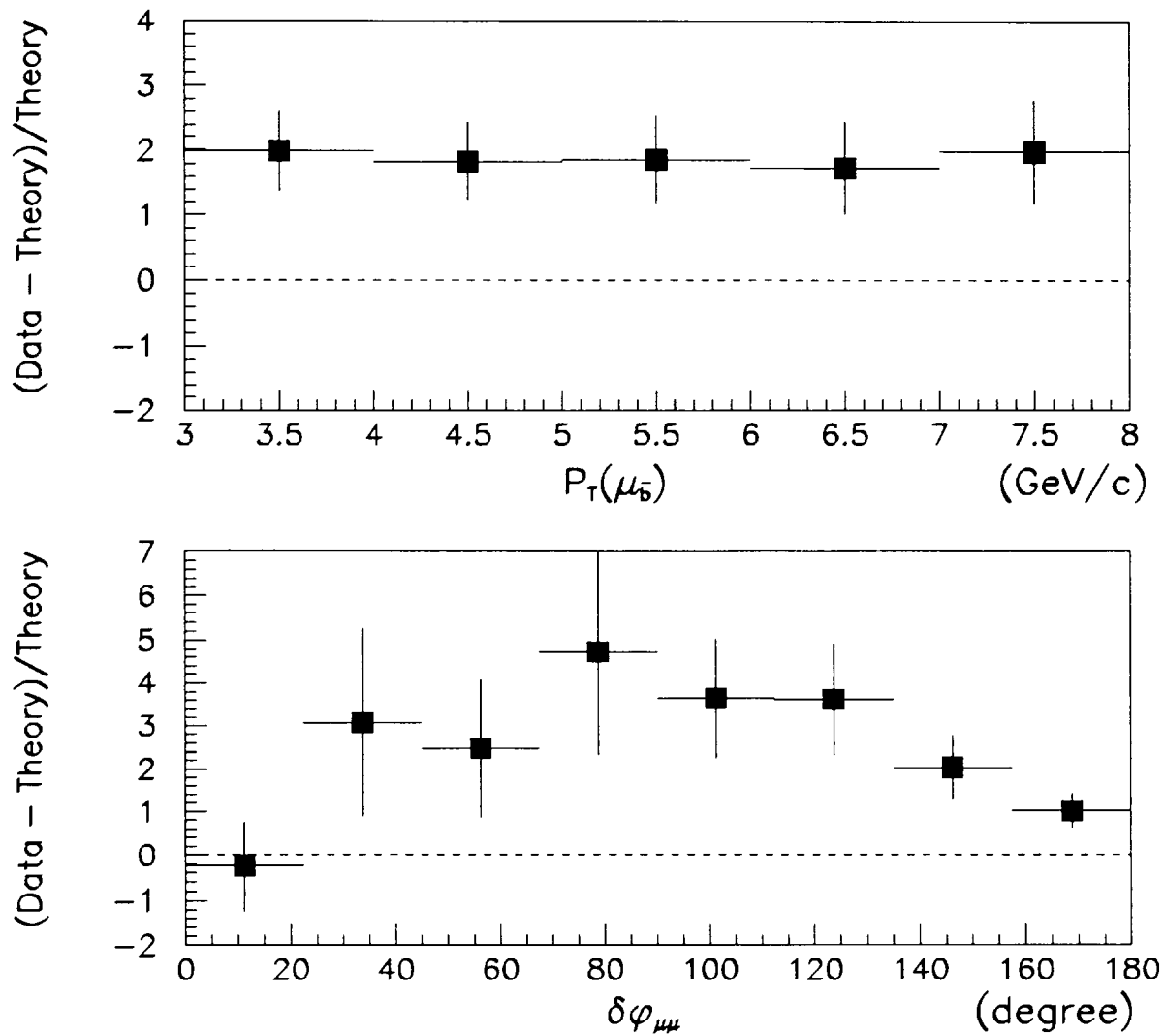


FIG. 9. $(\text{Data}-\text{Theory})/\text{Theory}$ distributions of $P_T(\mu_{\bar{b}})$ (top) and the opening angle between the muons in $b\bar{b}$ events (bottom). The uncertainties include the uncertainties of the data point and of the theoretical prediction.

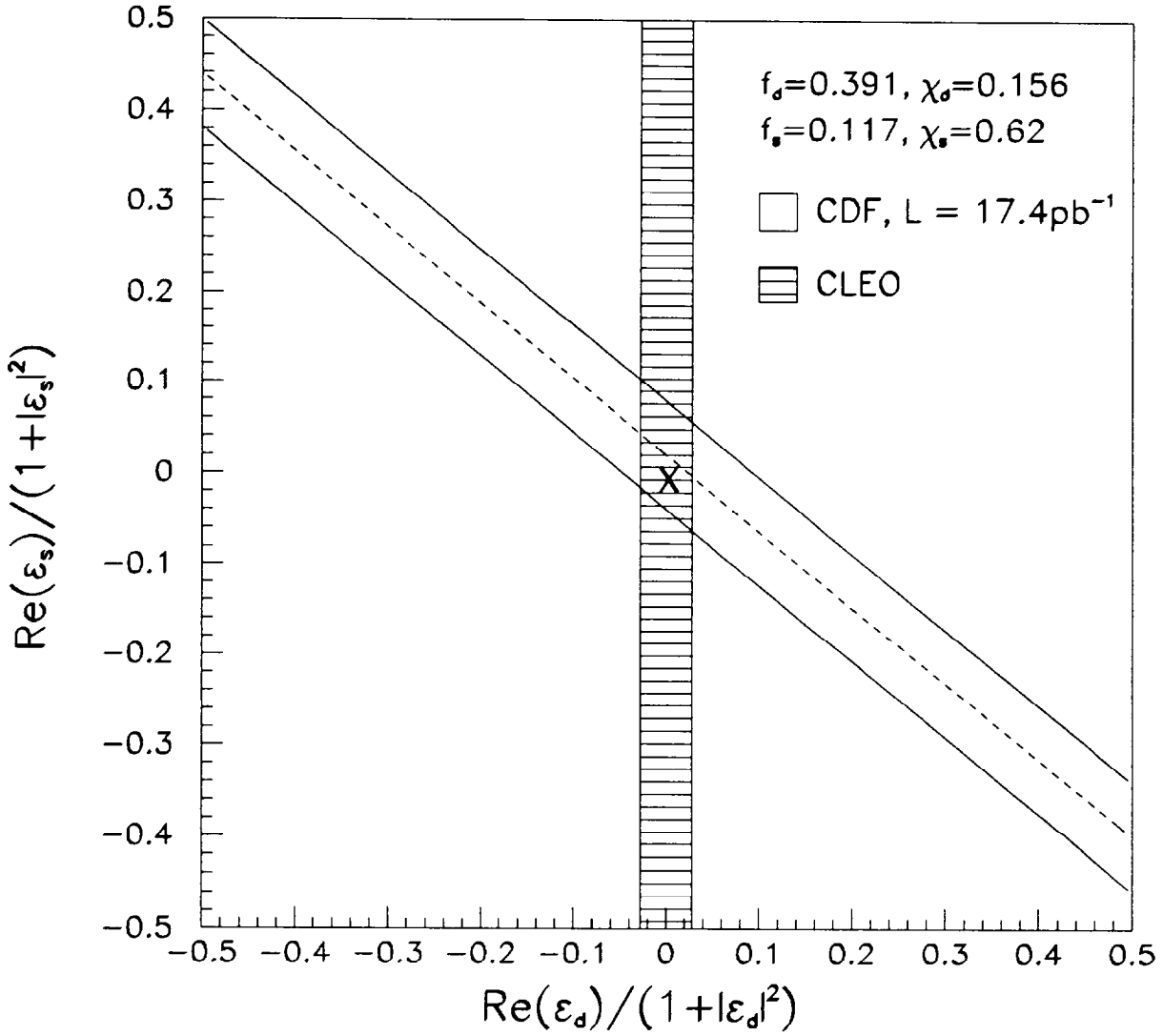


FIG. 10. The solid lines represent the $\pm 1\sigma$ uncertainties and the dashed line represents the measured value of the asymmetry. The hatched region is from the CLEO measurement in $B_d^0 \bar{B}_d^0$ sample. The marker X represents the prediction of the standard model.

TABLES

TABLE I. Systematic uncertainties of the fit

Source	Systematic Uncertainty (%)
B lifetime	$\pm 5\%$
resolution difference	$+7\%$
sequential fraction	$\pm 0.5\%$
prompt muons	$\pm 1.0\%$
charm muons	$\pm 4.7\%$
Total	$^{+9.9\%}_{-7.0\%}$

TABLE II. Efficiencies

$P_T(\mu_b)$	$\geq 3 \text{ GeV}/c$	$\geq 3 \text{ GeV}/c$	$\geq 3 \text{ GeV}/c$
$P_T(\mu_{\bar{b}})$	3 - 5 GeV/c	5 - 7 GeV/c	$\geq 7 \text{ GeV}/c$
Event vertex		0.742 ± 0.021	
CTC track finding		0.96 ± 0.02	
Muon identification		0.826 ± 0.044	
SVX track finding		0.669 ± 0.024	
Trigger	0.832 ± 0.037	0.847 ± 0.038	0.848 ± 0.038
Impact parameter cut	0.917 ± 0.006	0.925 ± 0.006	0.930 ± 0.006
Dimuon mass cut	0.906 ± 0.001	0.940 ± 0.001	0.952 ± 0.001
Combined Efficiency	0.272 ± 0.023	0.290 ± 0.025	0.296 ± 0.025

TABLE III. Integral $b\bar{b}$ cross sections and individual factors used in the cross section calculations

$P_T(\mu_b)$	$\geq 3 \text{ GeV}/c$	$\geq 3 \text{ GeV}/c$	$\geq 3 \text{ GeV}/c$
$P_T(\mu_{\bar{b}})$	$3 - 5 \text{ GeV}/c$	$5 - 7 \text{ GeV}/c$	$\geq 7 \text{ GeV}/c$
$N_{b\bar{b}}$	$1610 \pm 87(stat)_{-113}^{+160}(sys)$	$495 \pm 46(stat)_{-35}^{+49}(sys)$	$368 \pm 36(stat)_{-26}^{+36}(sys)$
Luminosity	$17.4 \pm 0.6 \text{ pb}^{-1}$		
Efficiency	0.272 ± 0.23	0.290 ± 0.025	0.296 ± 0.025
Acceptance	$(1.32 \pm 0.13) \times 10^{-2}$	$(0.55 \pm 0.05) \times 10^{-2}$	$(0.61 \pm 0.06) \times 10^{-2}$
$P_T^{min}(b)$	$6.5 \text{ GeV}/c$	$6.5 \text{ GeV}/c$	$6.5 \text{ GeV}/c$
$P_T^{min}(\bar{b})$	$6.5 \text{ GeV}/c$	$8.75 \text{ GeV}/c$	$12.25 \text{ GeV}/c$
$\sigma_{b\bar{b}}(\text{in } \mu\text{b})$	$2.42 \pm 0.13(stat)_{-0.42}^{+0.45}(sys)$	$1.68 \pm 0.15(stat)_{-0.29}^{+0.31}(sys)$	$1.10 \pm 0.11(stat)_{-0.19}^{+0.20}(sys)$

TABLE IV. Dimuon cross section as a function of $\delta\phi_{\mu\mu}$ and $P_T(\mu_i)$. The common systematic uncertainties ($^{+9.9\%}_{-7.0\%}$) of the fit and of the luminosity ($\pm 3.6\%$) are included in addition to the statistical error.

$\delta\phi_{\mu\mu}$ (degree)	Cross section (pb)
0-22.5	$0.11^{+0.19}_{-0.11}$
22.5-45	$1.26^{+0.57}_{-0.56}$
45-67.5	$2.25^{+0.81}_{-0.80}$
67.5-90	$6.72^{+2.60}_{-2.54}$
90-112.5	$9.48^{+1.87}_{-1.77}$
112.5-135	$19.94^{+3.00}_{-2.65}$
135-157.5	$38.40^{+4.87}_{-4.06}$
157.5-180	$64.19^{+7.48}_{-5.98}$

$P_T(\mu_i)$ (GeV/c)	Cross section (pb)
3 - 4	$58.39^{+7.07}_{-5.77}$
4 - 5	$33.64^{+4.09}_{-3.35}$
5 - 6	$18.03^{+2.79}_{-2.49}$
6 - 7	$11.01^{+1.92}_{-1.76}$
7 - 8	$6.92^{+1.46}_{-1.38}$